FINAL REPORT
to the
Development Testbed Center Visitor Program

Development of an HWRF Diagnostics Module to Diagnose Intensity and Structure Using Synthetic Flight Paths through Tropical Cyclones†

Jonathan L. Vigh*
NCAR† Research Applications Laboratory, Boulder, Colorado

October 13, 2014

1 INTRODUCTION

Forecasts from regional hurricane models may suffer significant degradation when the structure of the simulated storm departs markedly from the observed storm. To assess and identify the deficiencies that lead to structural errors, it is necessary to develop alternative verification and diagnostic approaches that go beyond the computation of errors and biases in track and intensity. The plethora of aircraft reconnaissance and research flights taken each year offer an opportunity to make direct comparisons between the kinematic and thermodynamic quantities in the observed storm and those in the modeled storm. In order to make such direct comparisons, the observations must be compared within a framework that is consistent with the model's resolution and simulated storm location.

This report outlines the development and application of a code set to implement the synthetic profiles[1] technique to evaluate the intensity and structure of simulated tropical cyclones (TCs) in operational and retrospective runs of the Hurricane WRF model (HWRF). To accomplish this goal, the various National Oceanic and Atmospheric Administration (NOAA) and Air Force Reserve (AFRES) flight level data for a

*Corresponding author address: Jonathan Vigh, National Center for Atmospheric Research, P.O. Box 3000, Boulder, CO 80307-3000; e-mail: jvigh@ucar.edu

†The National Center for Atmospheric Research is sponsored by the National Science Foundation.

[1] In this report, the term *synthetic profile* is used generically to refer to radial structure data that have been obtained by sampling through a storm along a generally straight path that passes near to or through the center along a radial. In the literature, the term *profile* can also be used to refer specifically to an *azimuthal-mean* profile (such a profile could be the average of several individual radial legs). This document does not use 'profile' in that sense unless specifically noted. Practically, this module has been developed to construct synthetic *radial legs*, which consist of a flight segment that either begins or ends in or near the storm center.

given storm are first standardized into a common Network Common Data Format (NetCDF) file. Because the simulated cyclone does not typically follow the actual path taken by the real cyclone, it is necessary to translate the observational data into coordinates relative to the moving center of the actual storm and then sample the model space along these transects in a frame relative to the center of the simulated storm. The resulting synthetic radial profiles of the model's simulated flight level and surface data can then be directly compared with the observed 1-Hz flight level once an appropriate spatial smoothing is applied. Likewise, the model's simulated surface wind field can be sampled and compared with observed surface wind data from Stepped Frequency Microwave Radiometer (SFMR). The resulting radial structure information can then be used to diagnose model errors for storm size, inner core kinematic and thermodynamic structure, and surface wind field distribution.

This final report describes the work that was undertaken to develop the synthetic profiles software module and also examines the potential to use the synthetic profiles technique for advanced diagnostics and verification. The report documents details of the approach that has been taken, shows tests from a suite of comparisons generated for Hurricane Sandy (2012), and offers recommendations for future enhancements and applications. This report is organized as follows. Section 2 describes how the flight level data are processed to obtain the data in storm-relative coordinates. Section 3 provides details of the methods used to implement the synthetic profiles technique. Results from Hurricane Sandy are presented in Section 4. Some concluding discussion and recommendations for future work are given in Section 5.

2 PREPARATION OF FLIGHT LEVEL DATA

Extensive efforts have been exerted to prepare the observational flight level data for use with the synthetic profiles approach. This work was undertaken both with the partial support of the Development Testbed Center Visitor Program (DTCVP) and with funding support from the Risk Prediction Initiative (RPI). This section describes characteristics of the flight level data and then discusses efforts to standardize the multitude of data formats, conduct quality control (QC) measures of the flight level data, translate the flight level data into a frame moving with the storm center, automatically parse the flight trajectories to obtain high quality radial legs, and then store the output in a regular binned radius coordinate. This section also details additional QC measures that have been undertaken on the SFMR surface data in order to get useful radial legs of surface wind speed. The result of this multi-step process is a high quality research-grade data set of flight level data, now known as the Extended Flight Level Data Set (or FLIGHT+). The FLIGHT+ data set is suitable for a multitude of research uses including dynamical process studies, data assimilation experiments, and wind risk applications. The FLIGHT+ data set may possibly be the most enduring and scientifically useful product arising from both the DTCVP and RPI projects.

2.1 Characteristics of flight level data

Flight level data are typically obtained from two sources: the Air Force Reserve (AFRES) and NOAA's Aircraft Operations Center (NOAA/AOC). AFRES flights are normally conducted in support of operational reconnaissance of storms that may pose a threat to land in the North Atlantic, Northeast Pacific, or Central Pacific basins. As such, these flights normally follow a typical figure-'4' pattern at standard flight levels (1500 ft, 925 hPa, 850 hPa, or 700 hPa). Occasionally, AFRES planes may participate in field campaigns in other TC basins around the world (e.g., the Western Pacific). Most AFRES data are provided at a temporal sampling rate of 10-seconds (during which time the plane flies approximately 1.2 km). Since 2010, AFRES data have been provided at a 1-second sampling rate. Prior to 2004, some flights are only provided at a 30-second sampling rate or occasionally at a 60-second rate. AFRES data are usually provided "as is" without substantial QC measures. The data files are made available on the Hurricane Research Division's (HRD)

web site. Especially in earlier years, it has been necessary to hand-edit some of the AFRES data files to remove erroneous blocks of data. AFRES data come in ASCII text format. Approximately six formats have been used over the period 1997-2013. On occasion, the original AFRES flight data are unavailable; in those cases, operational data files may be substituted [e.g., the older "Minob" or more recent 'High Density Obs' (HDOBS) formats]. On other occasions, complex measures have been required to handle certain formatting issues in the legacy data files (described in more detail in the next subsection).

Although NOAA Hurricane Hunter aircraft can also be tasked for operational reconnaissance missions, NOAA flights are often conducted in support of the annual hurricane field program or other field campaigns. Because the aims of such research flights often involve a different set of priorities than those of operational missions, NOAA missions often fly at non-standard flight levels (e.g., near 650 hPa) to maximize the utility of the airborne Doppler radar systems. Flight patterns may be irregular or contain many loops and cross-legs to maximize radar coverage of the storm. NOAA aircraft data are normally provided at a sampling rate of 1-second or 10-seconds, and are carefully QC'd by a flight meteorologist at AOC before being made available on HRD's web site. Since 2005, much of the NOAA flight data has been been provided in Network Common Data Format (NetCDF) files. Changes in variable naming over the years pose challenges to reading these data files, however the variable naming has become increasingly standardized. Prior to 2005, NOAA flight data are provided in ASCII text files. Like the AFRES formats, the NOAA formats have also varied over the years: approximately eight data formats have been used from 1997-2013.

2.2 Standardization of flight level data

In order to provide a high quality data set of flight level data suitable for comparing to model data, all available flight level data from 1997 to 2013 are standardized into a common data format. All of the AFRES and NOAA flight data from each storm are read and combined into one self-describing NetCDF file that uses a standardized set of variable names. When data were provided in English units, they have been converted into metric units. This standardized combined file is termed the *Level 1 (L1)* data product. One L1 data file exists for each storm in the data set. Generally, all variables that typically exist in *both* of the AFRES and NOAA data files have been included in the common standardized file. Details about the correspondence of variable names and units between the source data files and the standardized data file are provided at: https://wiki.ucar.edu/display/flight/Correspondence+of+Variables+Between+Raw+Data+Files+and+the+Common+Data+Format.

2.3 Quality control of flight level data

The RPI project has provided considerable support to QC the aircraft data in order to create a research-grade data set that can be used for wind-risk applications. To ensure that each data file has been read correctly, the flight level data for several key meteorological parameters have been plotted in earth-relative coordinates. Fig. 1 shows an example of such a plot for flight level wind speed for the final flight before Hurricane Sandy made landfall in New Jersey on 29 Oct 2012. Parameters that are plotted in this manner include the flight level pressure, flight level temperature, flight level wind speed, surface wind speed from the SFMR, and extrapolated surface pressure.[2] Working as part of the NCAR/RPI project, Christopher Williams checked each flight for artifacts or unrealistically high wind speeds. These checks are necessary because the underlying source data files from the NOAA HRD Hurricane Research Division (HRD) sometimes contain formatting errors that can result in the data being read incorrectly. When corrections were made to the source data files, a summary of changes has been noted on the dataset summary page: https://

[2]SFMR data have been routinely available on most flights since 2008. Flight level pressure is not available for many AFRES flights prior to 2005.

wiki.ucar.edu/display/flight/Summary+of+Flight+Level+Data+Processing+by+Storm (additional details of changes are described on the individual storm pages linked from that page). The resulting cleaned files have been sent to HRD to update the data files on their web page. Particular attention has been taken to ensure that the wind speed data are not affected by artifacts that lead to erroneously high maximum values. When the sources of such artifacts are found, the source data files have been edited to remove the offending data points. Other types of read errors have also been corrected when possible. A short description of some of the issues encountered and the subsequent actions that were taken are given below in Table 1.

2.4 Quality control of SFMR surface wind speed data

In the course of conducting quality checks of the flight level data, the NCAR/RPI Project Principal Investigator (PI, Jonathan Vigh) also created plots of the surface wind speed data from the Stepped Frequency Microwave Radiometer (SFMR). A vexing problem was discovered, in which numerous artifacts are present in the SFMR-retrieved surface wind speeds. Upon translation into storm-relative radial legs, these artifacts manifest as spikes (often exceeding $100\,\mathrm{m\,s^{-1}}$) or 'drop-outs' in which the SFMR-reported wind speed drops to zero or an unrealistically low value. The causes of these artifacts are not readily apparent, however, there do seem to be some systematic causes. Some of these systematic causes include:

- SFMR retrievals when the aircraft was flying over shallow water,
- retrievals when the aircraft was over land, and
- retrievals when the aircraft was rapidly changing its heading (e.g., turning at the outer termination points of radial legs).

To examine the sensitivity to the each of these factors, the PI created plots of SFMR wind speeds overlaid upon bathymetric depth obtained from the ETOPO1 data set Amante and Eakins (2009). This allows one to evaluate how the quality of the retrieved wind speed decreases as the depth decreases as well as to visually ascertain where the other artifacts occur with respect to the flight pattern. Three cases were selected, comprised of flights where the TC travelled over regions of shallow water adjacent to complex coastlines: Ike near Cuba (2008, see Fig. 2), Fay near the Florida coast (2008, see Fig. 3), and Irene over the Bahamas (2011, see Fig. 4).

Figure 2 shows retrieved SFMR wind speeds for Ike (2008). The retrieved wind speed values are obviously erroneous over land, and they are also suspect in the region between the main island of Cuba and the Isle of Youth where the water depths are very shallow ($< 5\,\mathrm{m}$). Erroneous retrievals over land are to be expected since the physics behind SFMR retrieval require that an ocean surface be present. Faulty retrievals over shallow water are also to be expected. This is due to the following: the SFMR senses the wind speed by measuring the differences in microwave radiation upwelling from the ocean surface at various frequencies. Since the emission of microwave radiation is highly dependent on the amount of sea foam present due to breaking ocean waves, areas of shallow water depth lead to waves that have different shoaling and breaking characteristics than waves in the deep ocean and hence, the SFMR retrieves a wind speed which is incorrect. This shallow-water-retrieval effect cannot be clearly seen in this example however, since the western leg crosses from deep water into very shallow water ($< 2\,\mathrm{m}$ depth) without much apparent change in retrieved wind speed. The wind speeds have large errors near the storm center in the shallow water regions in this case, which may have something to do with the broad directional spectra of the wave field near the wind center of the TC. Additional artifacts can be seen at the leg turn points, as indicated by small white line segments. In these regions, the retrieved wind speed incorrectly decreases to very low values because the SFMR instrument is not pointing to nadir – when not pointing straight downward, another assumption of the retrieval algorithm is violated, since the radiation is now arriving at the plane's location after following a slanted path. Finally, additionally questionable wind speed retrievals can be seen on the flight segment

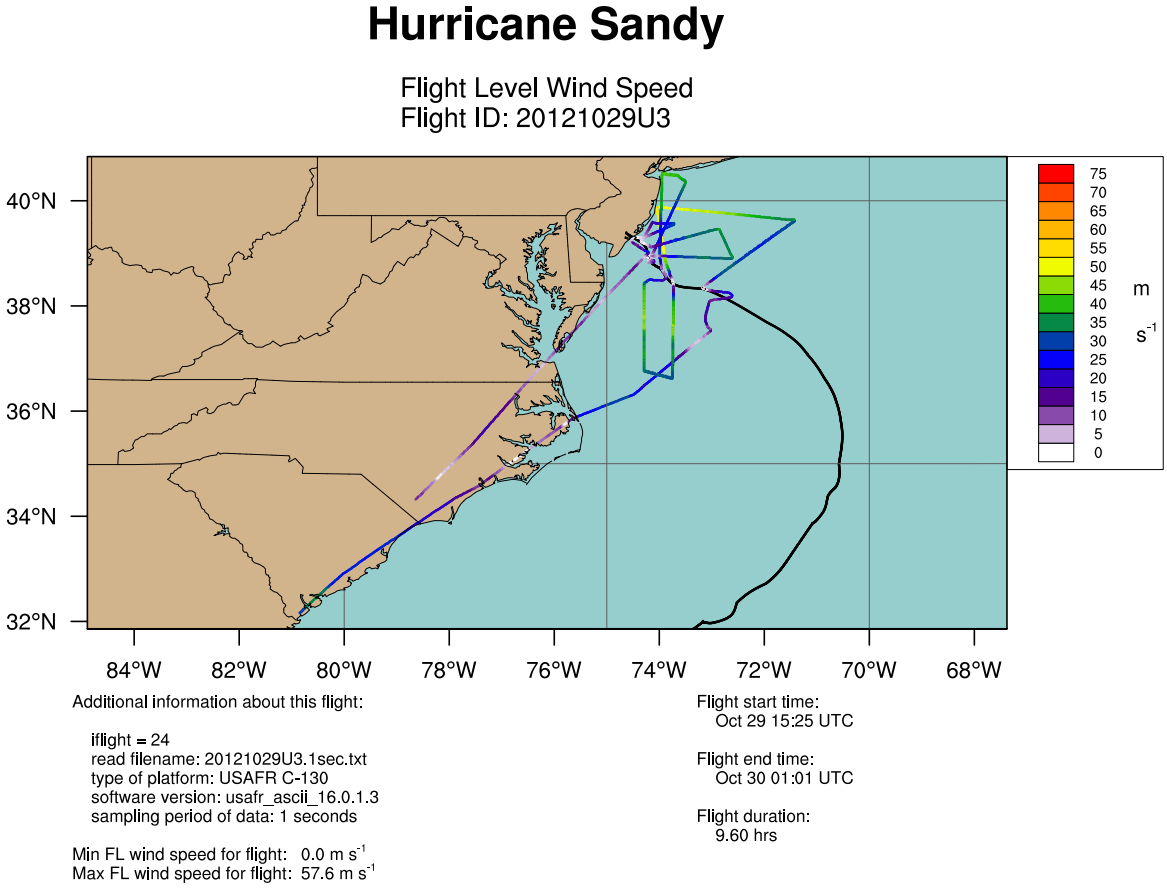

Figure 1: Flight level wind speed plotted in earth-relative coordinates for the final flight before Hurricane Sandy made landfall in New Jersey. The flight began at 15:25 UTC on 29 Oct 2012 and ended at 01:01 UTC on 30 Oct 2012 – near the time that Sandy made landfall. Flight level wind speed along the flight trajectory is indicated by the color of the line; the black line shows the path taken by the center the storm as determined by the wind-center-finding method of Willoughby and Chelmow (1982).

Test2 (2008)

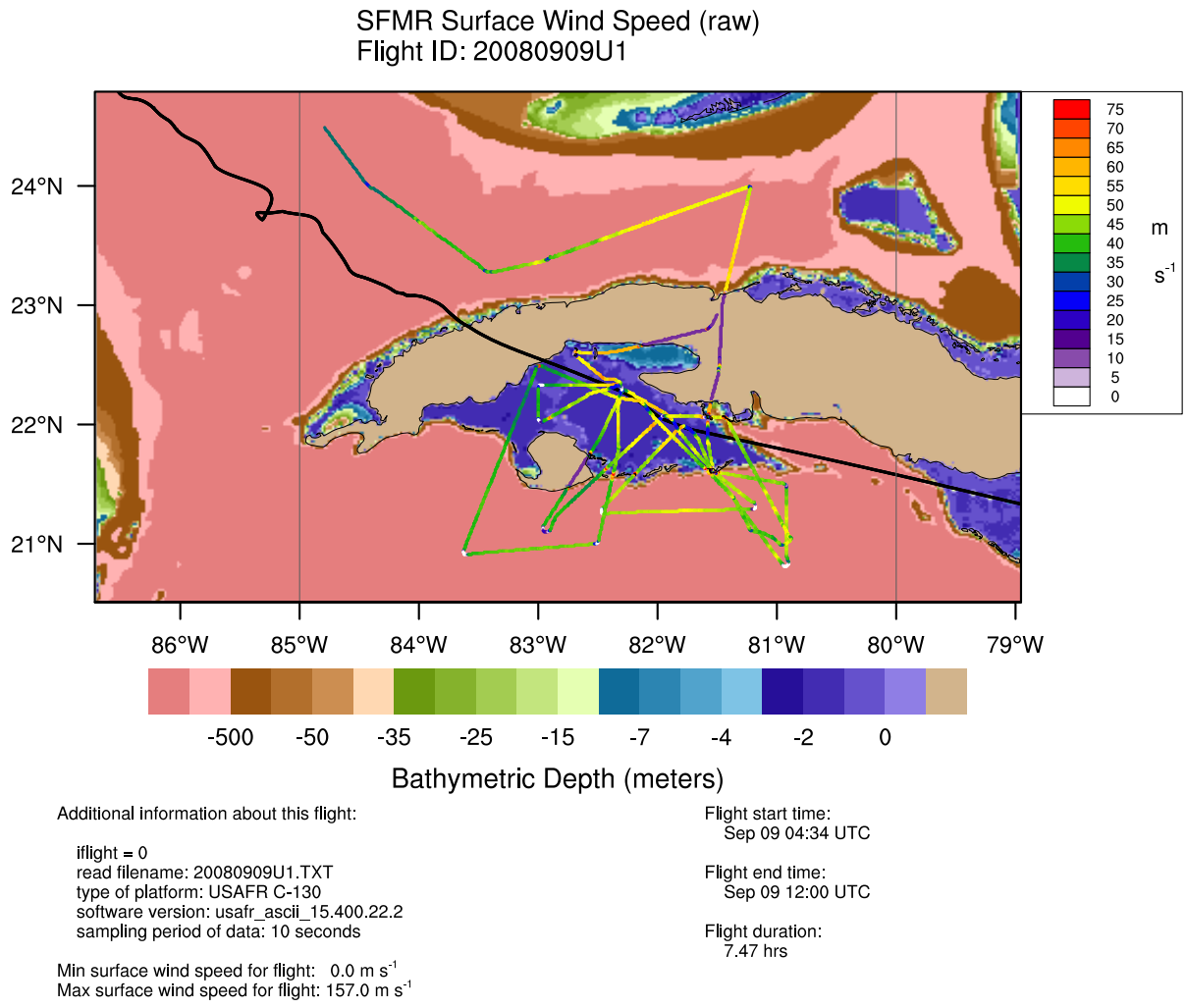

Figure 2: Retrieved SFMR surface wind speeds without any additional quality control measures (lines colored by retrieved wind speed) plotted atop bathymetric depths (color shading) from the ETOPO1 data set for Ike (2008). Note that the scale for bathymetric is highly nonlinear in order to emphasize gradients in shallow water. The black line shows the track of the storm, as determined by wind centers obtained from the Willoughby-Chelmow center finding method.

Table 1: Example of quality control issues and actions taken during the visual checks of the earth-relative flight level wind data. Table by Christopher Williams, courtesy of the RPI project.

Summary of Problems Encountered with Data Files and Measure Undertaken to Correct	
Issue	Action
Unrealistically high flight level wind speed values (e.g., 80 m s^{-1} in a tropical storm or weak hurricane)	Inspect data file. If unreasonable, change wind speed value to missing value (-99); if many values are bad, then remove block of data with high wind speeds
Odd flight duration/date/time stamp non-sequential or time stamp jumps	Change date/time stamp of affected lines or delete block of data if duplicate time information is present
Unrealistic latitude/longitude values or location jumps	Change lat/lon to correct values (if apparent) or delete block of data with bad lat/lon values
Data file missing a column in certain lines	Delete block of data with missing column data
Data file has extra 1's in a column right after the date, causing mis-translation of subsequent columns	Clean using clean˙bad˙column.ncl to remove superfluous 1's

north of the island, where unrealistically high values are present far from the storm center, along with several areas with rapid variations over a short distance. The maximum retrieved SFMR wind speed for this flight was 157 m s^{-1}.

Figure 3 shows a similar plot for Hurricane Fay (2008). In addition to the artifacts noted for the previous case, additional artifacts are present including unrealistically high wind speeds regardless of water depth and abnormal variability of wind speeds just east of the southeast Florida coast. This first additional artifact suggests that the SFMR instrument may have been poorly calibrated for this flight, leading to questionable retrievals for the entire flight. The latter artifact may be related to the rapid current and associated variations in wave characteristics and surface temperatures of the Gulf Stream. The maximum retrieved SFMR wind speed for this flight was 140 m s^{-1}.

Figure 4 shows a similar plot for Irene (2011). Compared with the previous two cases, this case looks fairly well behaved, with the normal artifacts over land and at the turn points. The effect of shallow water is not readily seen here. The maximum retrieved SFMR wind speed for this flight was 88.5 m s^{-1}.

The presence of pervasive artifacts in the SFMR-retrieved wind speeds represents a significant obstacle to the goal of comparing the observations of surface wind speed to those of the model. Thus, considerable effort has been undertaken to devise methods to screen out these erroneous wind speed values while preserving the high quality surface wind speeds. A data quality mask has been implemented at the initial processing stage to account for known causes of retrieval errors. Th procedure for setting this data quality flag is described in the following paragraphs.

At the beginning of the QC process, the SFMR data quality flag is assigned a value of zero for all points along the flight trajectory. A value of zero indicates that no QC screening criteria have been applied and thus, the quality of the retrieved wind speed is expected to be comparable to the quality of retrievals over deep-sea conditions. Next, a water depth criterion is used to increment the value of data quality flag by one for each location in which the water depth is less than the given threshold. This is accomplished by retrieving the bathymetric water depth from the ETOPO1 dataset for each point along the flight trajectory. The ETOPO1 data set has a horizontal grid spacing of approximately 1.3 km, which closely matches the characteristic horizontal scale of the surface footprint of the SFMR instrument when flying at typical reconnaissance altitudes (e.g., 850 and 700 hPa). For each point along the flight trajectory, the depth is retrieved for the grid cell closest to the point directly beneath the plane's location. Since slight variations in the plane's roll angle

Test3 (2008)

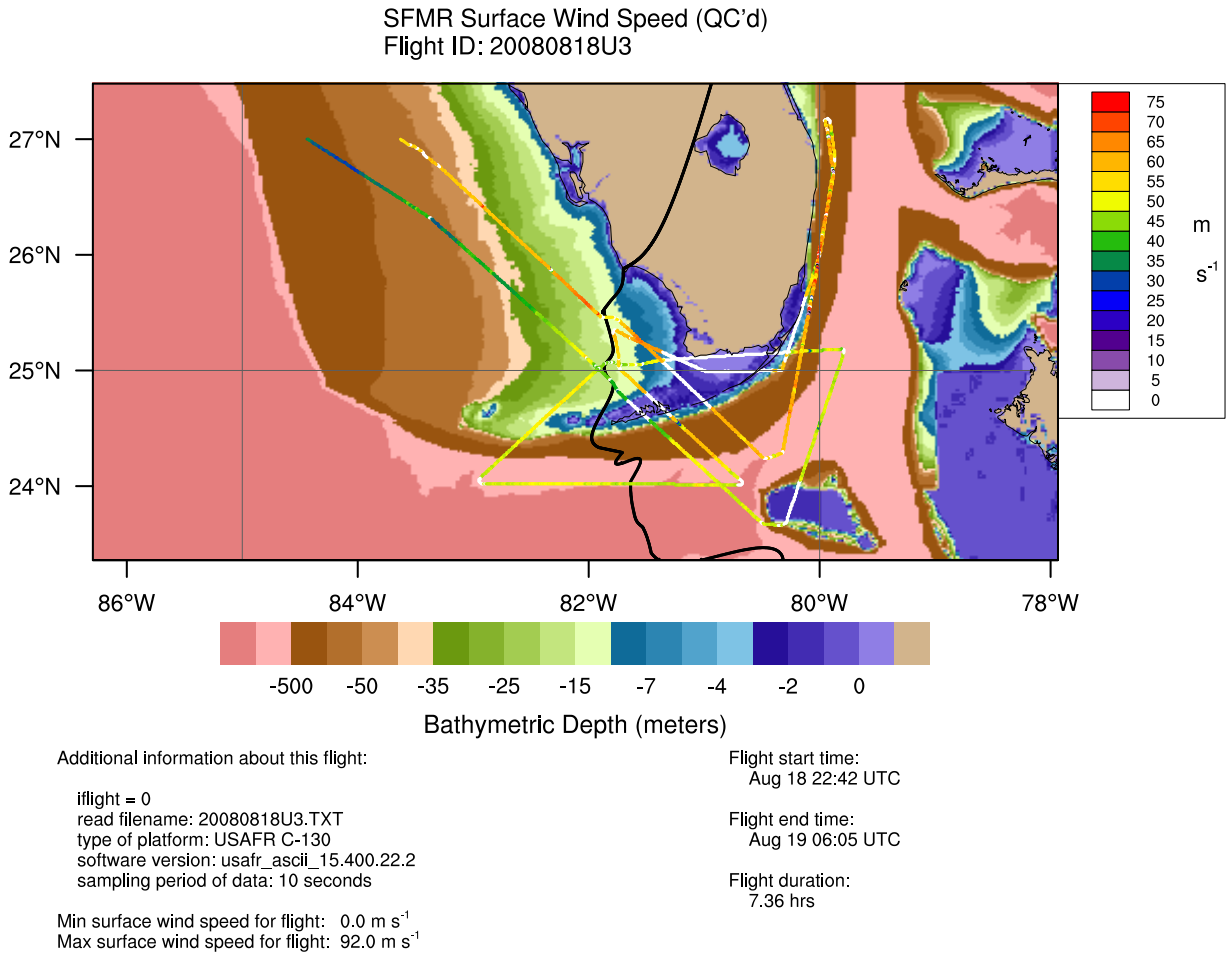

Figure 3: As in Fig. 2, but for Hurricane Fay (2008).

Test1 (2011)

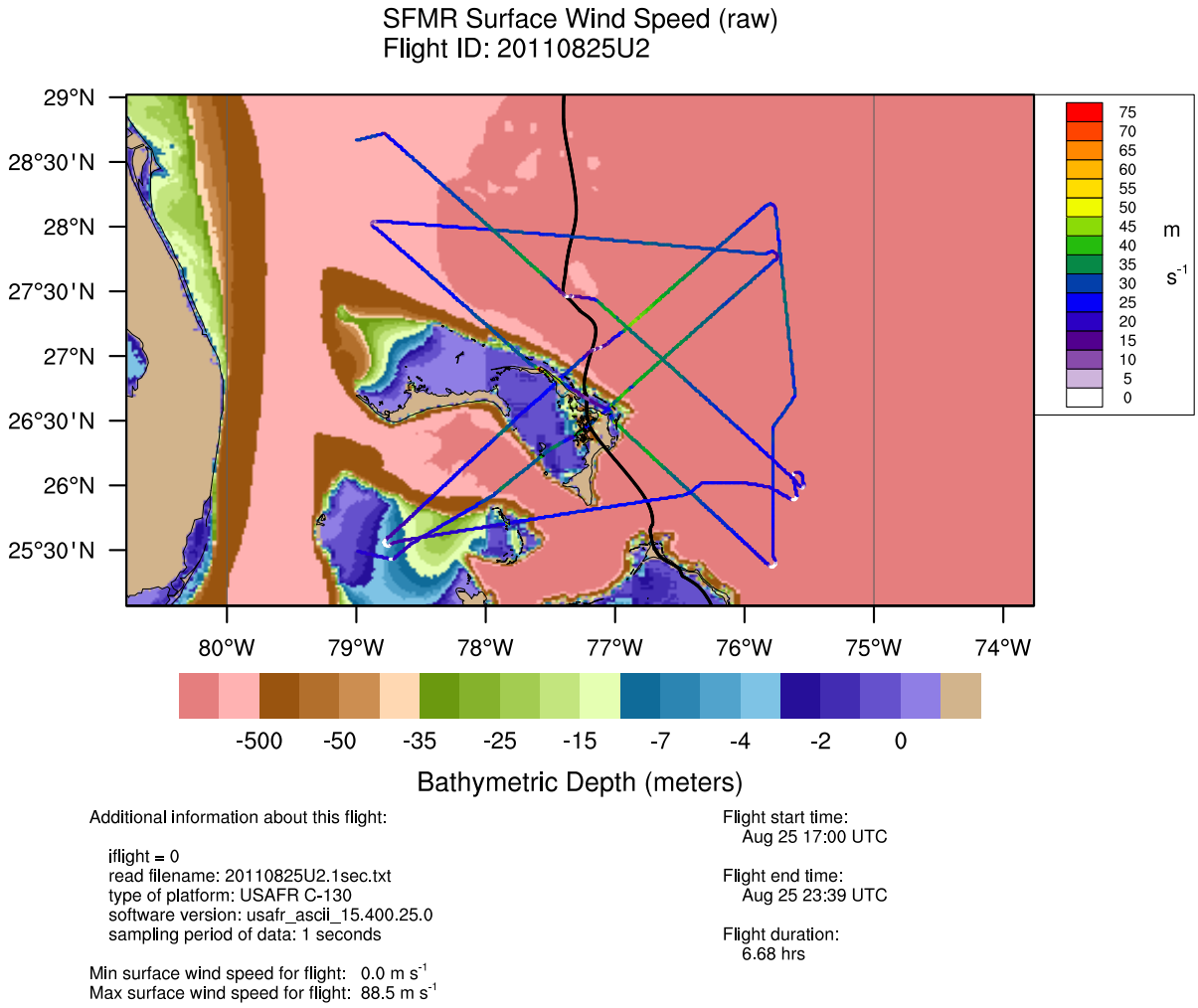

Figure 4: As in Fig. 2, but for Hurricane Irene (2011).

could result in the SFMR footprint falling on nearby ocean points rather than the point directly beneath the plane, water depths are also retrieved for the nearest grid cells north, east, south, and west of the point directly beneath the plane. If the shallowest of these five depths is not deeper than 5 m, the data quality flag is incremented by a value of unity. This effectively masks out most artifacts related to shallow water. Since the ETOPO1 dataset also includes altitude above sea level for land, this criterion also screens out any retrievals that were made over land.

The second QC criterion checks whether the plane was rapidly changing direction at each point along the trajectory. Since planes typically bank during turns, a rapid change in direction is a good indication that the SFMR was not pointing at nadir. The absolute rate of change in the plane's direction is computed by taking a one-point backward difference of true heading at each point along the flight trajectory, and then dividing by the elapsed time between points. For any trajectory points for which the plane's heading was changing by more than two degrees per second, the value of the data quality flag is incremented by a value of two.

The third QC criterion checks whether the plane was rolling at each point along the trajectory. If the value of the roll angle exceeds two degrees, then the data quality flag is incremented by a value of four.[3] Because the data quality flag values are additive and incremented by distinctly different amounts, it is possible to decode the data flag value to determine which combination of factors resulted in the point being flagged to indicate potentially poor quality.

The results of the QC'd SFMR wind speeds are shown in Figures 5-7. Fig. 5 illustrates the effects of these QC procedures – one can see that the data quality flag does indeed mask the wind speeds over land and shallow water, resulting in the elimination of many of the artifacts. Additionally, the rate-of-change/roll angle criteria have resulted in the elimination of low wind speeds at the turn points. This has also reduced some of the spurious variability in the northern leg, which was apparently due to the plane rolling during relatively straight flight (such rolls can occur due to turbulence). Fig. 6 shows that these QC criteria are not able to correct the issue of high variations in retrieved wind speed over the Gulf Stream, and they also do not correct the general problem of poor calibration. Fig. 7 shows that a number of short segments were screened by the roll angle criterion even during segments of straight flight.

To further illustrate the effectiveness of the QC measures, panel plots of the radial legs are shown for these three cases in Figs. 8-10. Each panel contains wind speed data translated into radial legs relative to the storm center. The top panel shows the flight level wind speed, the middle panel shows the non-QC'd SFMR wind speeds, and the bottom panel shows the QC'd SFMR wind speeds. All of the radial legs in this plot were flown at 700 hPa.

Figure 8 shows the panel plot for Ike. For this case, the QC measures are able to eliminate most of the spurious spikes and dropouts. The SFMR surface wind speeds are generally higher than the flight level wind speeds at all radial points; this suggests that the SFMR had poor calibration for this flight. The QC measures result in a reduction of the maximum SFMR wind speed from 157 $\mathrm{m\,s^{-1}}$ to 119 $\mathrm{m\,s^{-1}}$, while the minimum SFMR wind speed has increased from 0.0 $\mathrm{m\,s^{-1}}$ to 32 $\mathrm{m\,s^{-1}}$.

Figure 9 shows a similar panel plot for Fay (all of the radial legs in this plot were flown at 850 hPa). In this case, the QC measures are able to eliminate nearly all of the spikes upward, but a couple of prominent spikes downward remain. As in the previous example, this flight also suffered from poor calibration of the SFMR instrument, with unrealistically high SFMR wind speeds occurring at all radii. The QC measures result in a reduction of the maximum SFMR wind speed from 140 $\mathrm{m\,s^{-1}}$ to 92 $\mathrm{m\,s^{-1}}$; this is still unrealistically high, but apparently does not occur in any of the good radial legs. The minimum SFMR wind speed remains unchanged at 0.0 $\mathrm{m\,s^{-1}}$.

[3] Many flights from the 1990s and early 2000s do not contain the roll angle parameter, so the previously described rate of directional change criterion serves as a useful proxy for determining when significantly non-zero roll angles may have occurred.

Test2 (2008)

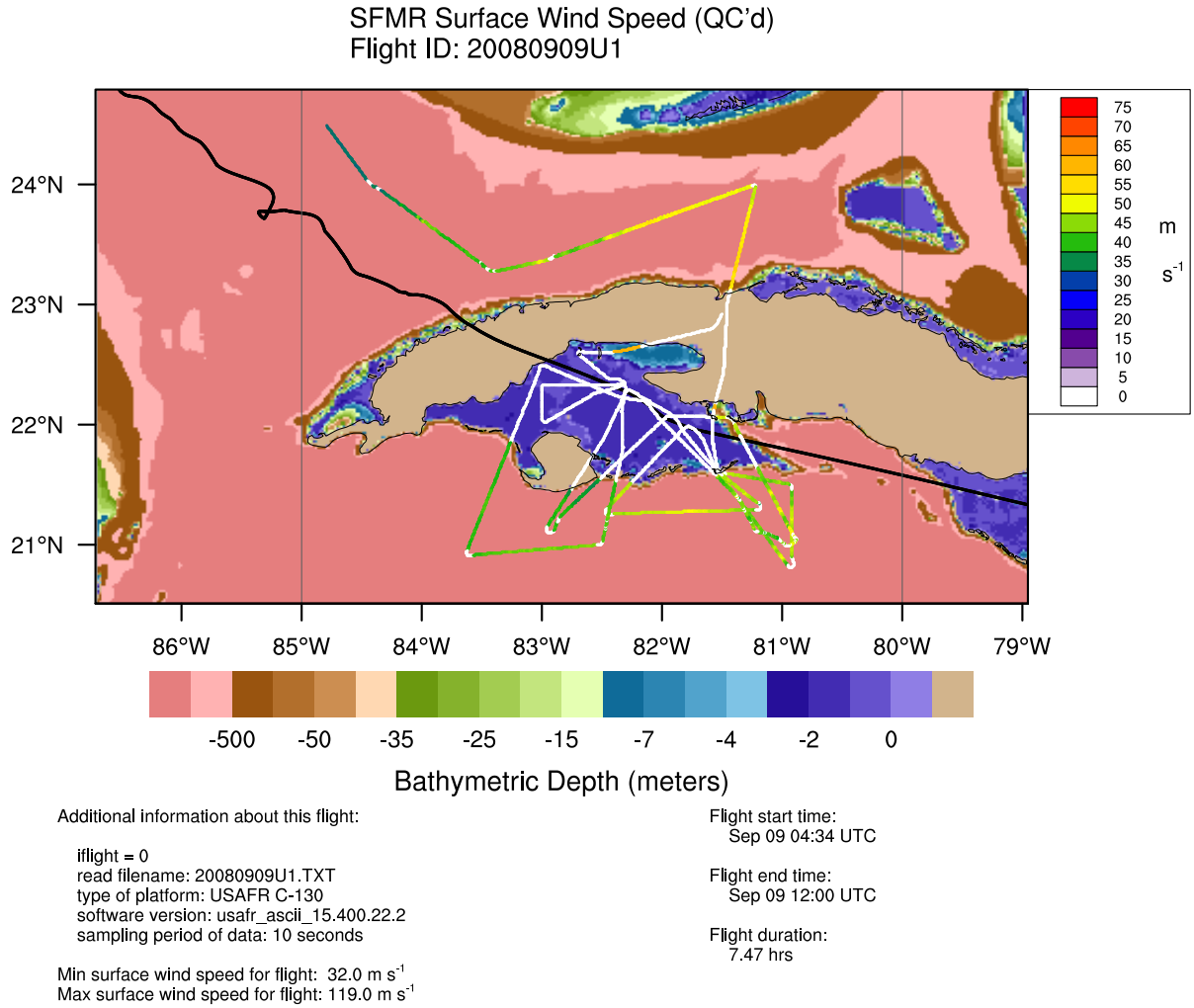

Figure 5: As in Fig. 2, but now showing the SFMR wind speed values that have undergone QC measures to screen out values over land, shallow water, or when the plane was turning rapidly.

Test3 (2008)

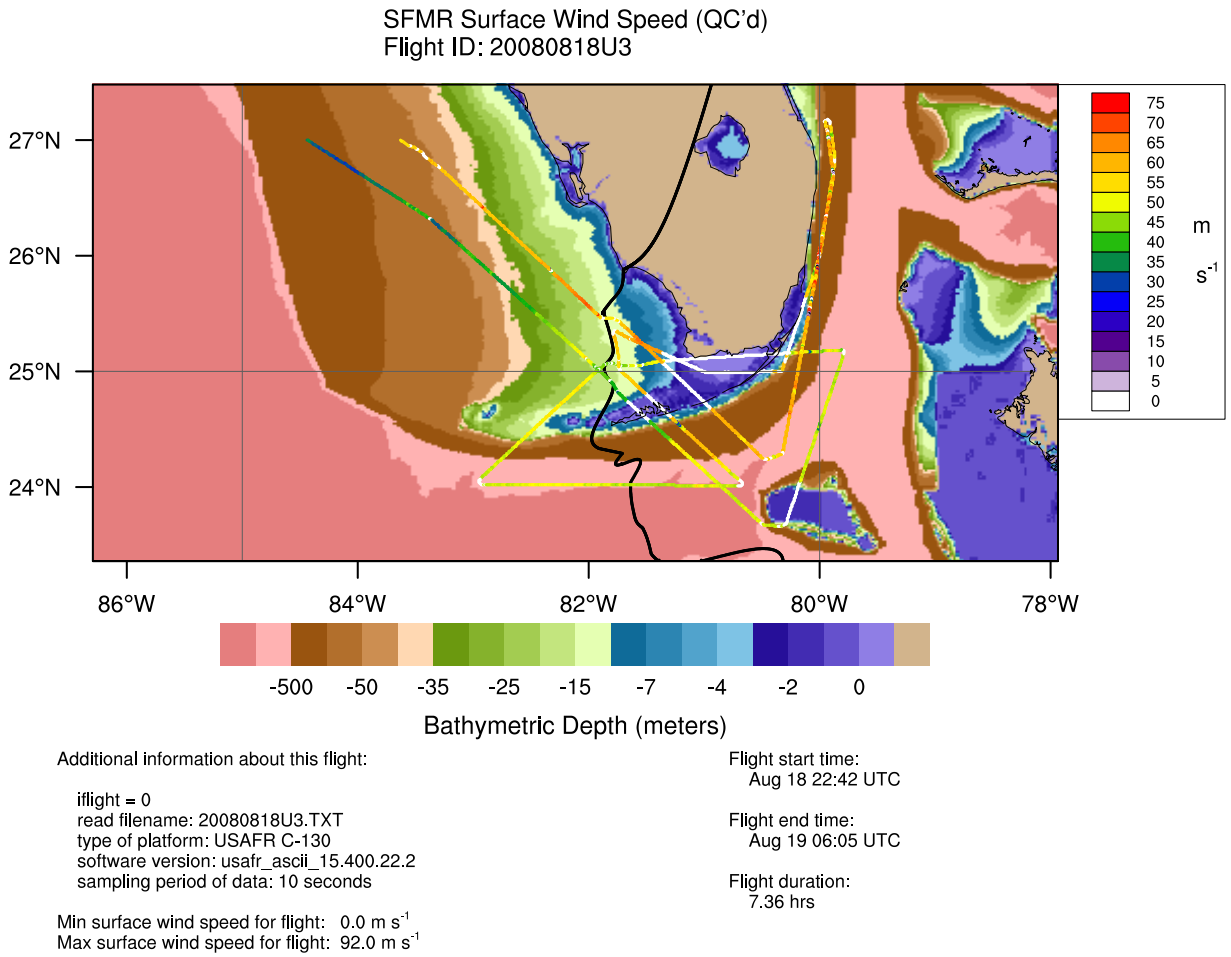

Figure 6: As in Fig. 3, but now showing the SFMR wind speed values that have undergone QC measures to screen out values over land, shallow water, or when the plane was turning rapidly.

Test1 (2011)

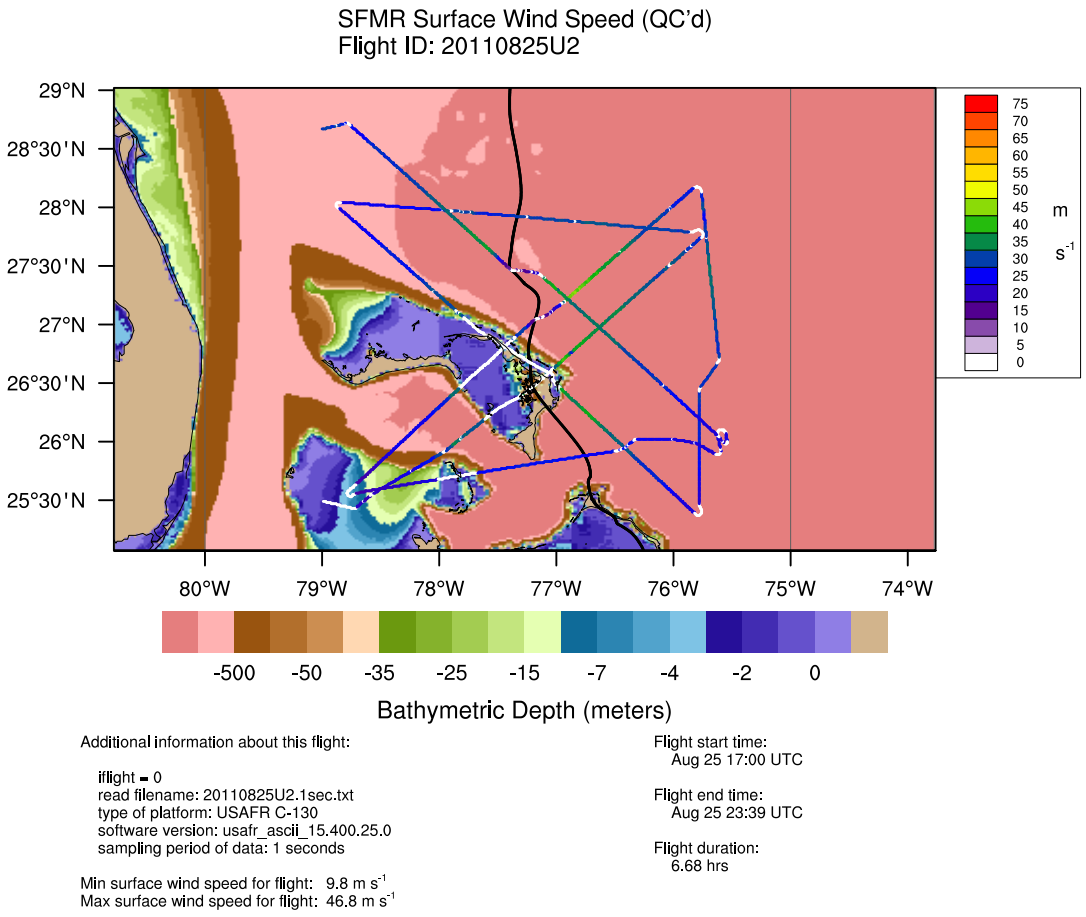

Figure 7: As in Fig. 4, but now showing the SFMR wind speed values that have undergone QC measures to screen out values over land, shallow water, or when the plane was turning rapidly.

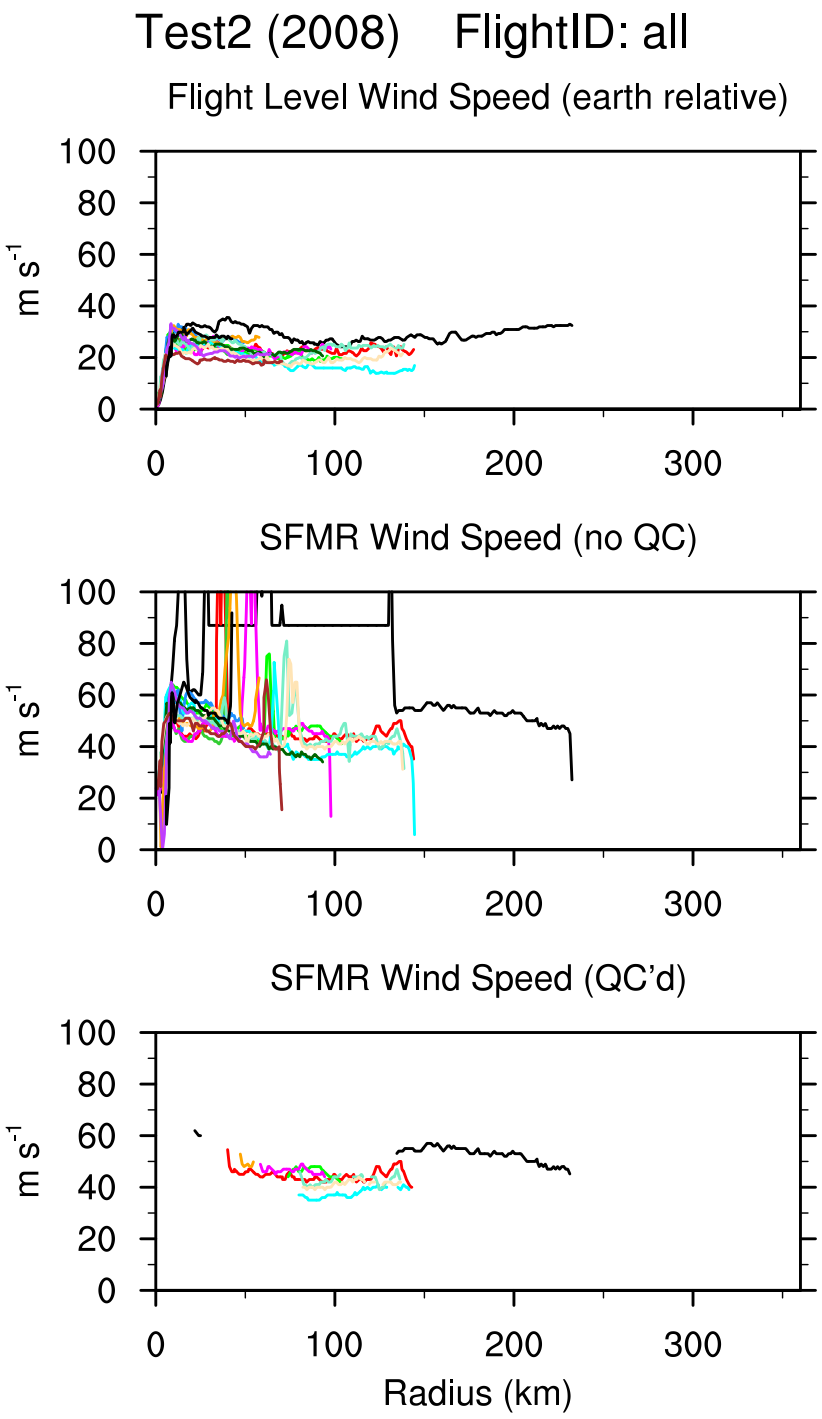

Figure 8: Panel plot showing the wind speeds for all of the radial legs in a particular flight for Ike (2008). Parameters shown are: flight level wind speed (top), non-QC'd SFMR wind speed (middle), and QC'd SFMR wind speed (bottom). All radial legs in this plot were flown at 700 hPa.

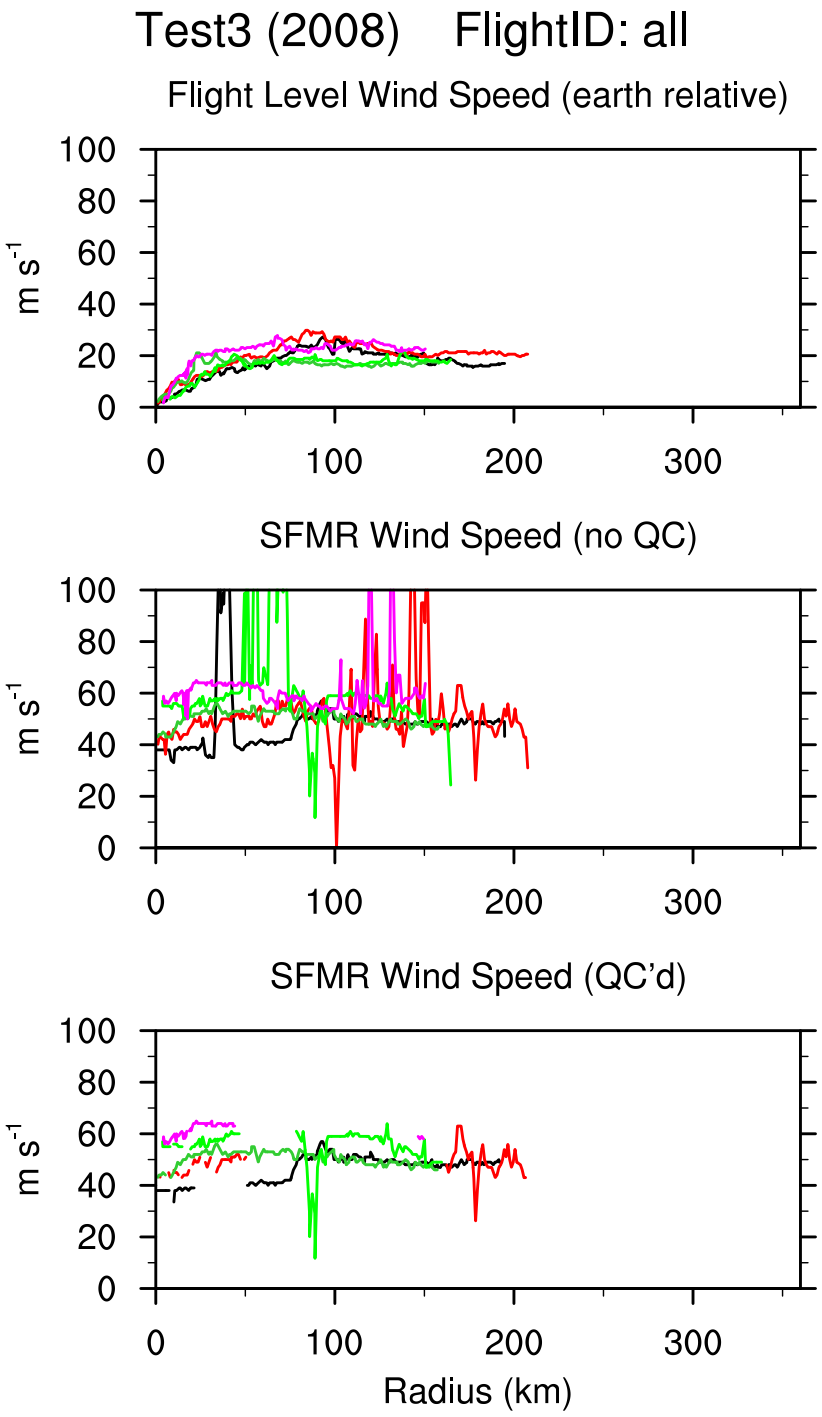

Figure 9: As in Fig. 8, but for Fay (2008). All radial legs in this plot were flown at 850 hPa.

Figure 10 shows the panel plot for Irene (all of the radial legs in this plot were flown at 700 hPa). In this test case, the QC measures eliminate all of the spikes and all prominent dropouts. One minor downward spike remains, but overall the SFMR radial legs of surface wind speed are very clean and correspond well with the radial legs of flight level wind speed. The QC measures reduce the maximum SFMR wind speed from 88.5 m s^{-1} to a realistic 46.8 m s^{-1}, while the minimum SFMR wind speed increases from 0.0 m s^{-1} to 9.8 m s^{-1} (also realistic). This case suggests that so long as the SFMR instrument was properly calibrated, it may be possible to obtain high quality radial legs of SFMR wind speed that are suitable for fitting to a parametric wind model.

2.5 Automatic parsing of radial legs

The next step in the data processing is to translate the flight level data into storm-relative coordinates. In order to do this, a detailed track of the storm center locations is required. HRD accomplishes this by running the wind-center-finding method of Willoughby and Chelmow (1982). The full method determines the wind center of the storm using lines normal to the wind at the aircraft's location and then through iteration, chooses the center that minimizes a cost function based on both wind and pressure information. The resulting wind centers are then fitted to a cubic spline under tension, resulting in a high quality track of the storm's wind centers in time. HRD's process for creating wind center tracks uses the first-guess centers from the Willoughby-Chelmow method, but then rather than iterating, a scientist manually picks out the centers that look reasonable and then a spline is fitted to produce the track. The end result is a file that contains the wind centers every two minutes for the times when aircraft were in the storm. This project downloads these wind center '.trak' files from HRD and uses those data to translate the flight level data into storm-relative coordinates by subtracting the geographical coordinates of the wind centers from those of the coordinates of the flight level trajectory. The motion of the storm center can also be subtracted from the wind speed, resulting in wind data that are in a frame moving with the storm center. Finally, the wind data are decomposed into tangential and radial wind components.

Once the data are in storm-relative coordinates, an automated algorithm is used to determine which parts of the flight trajectory correspond to "good" radial legs (i. e. subsets of data that represent a relatively direct transact through the storm center). The algorithm accomplishes this task by means of a filtering operation, in which all points that do not correspond to inbound or outbound points of a radial leg are masked out by setting accompanying data flags to 'missing'. In brief, three criteria are applied in this masking operation: (a) the distance from the storm center, (b) the radial motion of the plane, (c) and the direction that the plane is heading. First, all points that are more than 400 km from the storm center are eliminated from consideration to reduce the scope of the search (normally, radial legs initiate and terminate approximately 200 km from the storm center). Then, a radial motion criterion is applied by examining whether the aircraft's distance to the center is increasing or decreasing in time. Points along the flight trajectory where the aircraft's distance to the center is decreasing in time are marked as potential starting points for an inbound leg. Similarly, points at which the platform's distance to the center are increasing in time are marked as potential starting points for an outbound leg. All other points are eliminated from consideration for the starting points of inbound or outbound radial legs. Then, a directional criterion is applied by using the angle difference between the plane's track (the direction in which the plane is moving) and the radial that passes through the storm center. All points at which the plane is tracking in a direction that is within $\pm 35^\circ$ of the storm center are included as potential starting or stopping points for the radial legs; all other points are eliminated. Because the plane does not always pass through the direct center, some leeway is given in applying the radial motion and directional criteria. These are not applied when the plane is closer than 30 km (for the radial motion criterion) or 25 km (for the directional criterion) of the storm center.

Once all points that do not correspond to inbound or outbound radial legs have been screened out, the beginning and ending times of candidate radial legs are recorded. Then each leg is screened using

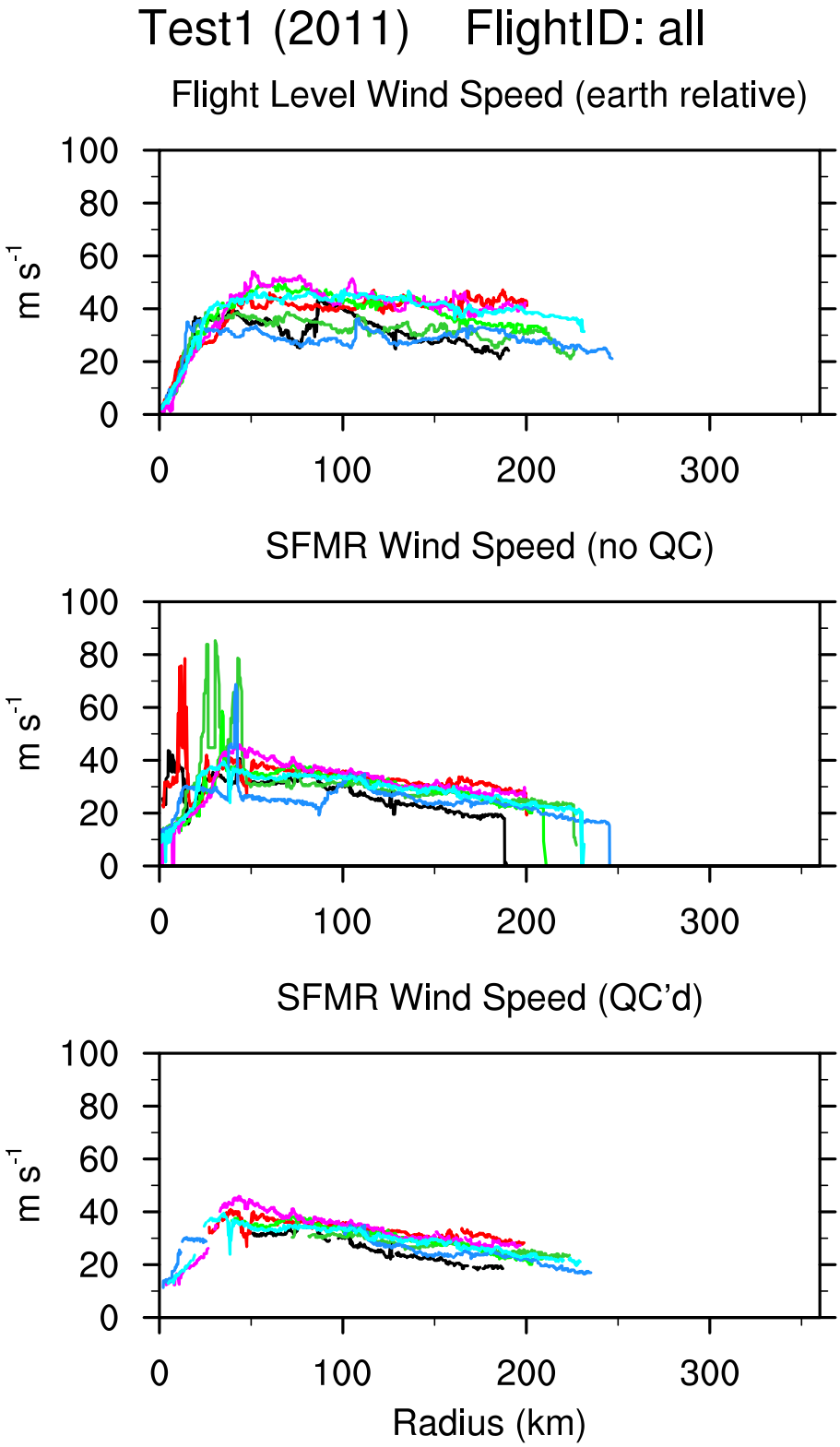

Figure 10: As in Fig. 8, but for Irene (2011). All radial legs in this plot were flown at 700 hPa.

additional criteria to see if it should be included as a 'good' radial leg. These additional criteria are: (i) that the continuous leg be at least 45 km in length, and (ii) that the plane pass within 25 km of the storm center. If both criteria (i) and (ii) are not satisfied, the leg is not included as a 'good' radial leg. Fig. 11 shows the result of the automatic parsing for the final flight before landfall in Hurricane Sandy. For this case, the algorithm correctly identifies the legs that are relatively straight and which pass near the storm center. Legs that are too short, that have too many directional changes, or which are not headed toward or away from the storm enter are correctly screened out. Overall, the algorithm correctly identifies good radial legs with an accuracy rate of about 99%. The parsing metadata is stored in a file for internal use, termed the *Level 2 (L2)* data product.

2.6 Radial binning

Once the 'good' radial legs have been identified, it is a rather simple exercise to take the parsing metadata from the Level 2 file for each storm, translate all of the earth-relative data into storm relative data, and then store the data into logical blocks that correspond to each radial leg. To allow ease of use in further applications, such as synthetic profiles, the data are then linearly interpolated (e.g., 'binned') from time/distance-from-the-center space into radius space using a common radial grid that starts at the storm center and extends outward to 700 km at 100-m grid increments. Given an assumed ground speed of 115 m s^{-1}, for 1-second data this results in a little less than one time point per radial point. For lower sampling rates, the linear interpolated (i.e., binned) data offers a very faithful radial representation of the data in the time domain. At a 1-second sampling rate, the linear interpolation may underestimate the maximum wind speeds of the most peaked wind profiles by a very small amount that should be less than the inherent uncertainty of the observations. To illustrate the effect of binning, Fig. 12 plots the binned (red curve) and unbinned (black curve) data for a radial leg in Hurricane Wilma on 19 October 2005.[4] As the reader can see, there are only a few places where any discernible difference can be seen between the two curves, and any differences are likely less than 0.5 m s^{-1}.

An additional QC measure is applied to the 'good' radial legs at this stage. Because it is possible that the plane may climb or descend during a radial leg (especially during the final leg leaving the storm), it is important to exclude any portions of the radial leg that are at a substantially different pressure altitude. This is accomplished by computing the average pressure of the leg within 25 km of the center of the storm. If the flight level pressure subsequently varies by more than 10 hPa from this value, the remainder of the leg is terminated (remaining values are set to `_FillValue` from this radius point outward). This QC criterion assures that changes in the flight parameters are not due to large altitude changes of the measuring platform. Fig. 13 shows the radial legs that result for the final flight before Sandy's landfall in New Jersey. Besides providing a qualitative overview of the radial leg data, the third panel of this 4-panel plot demonstrates that the radial leg truncation QC measure has indeed correctly terminated the northeast leg of Sandy. The earth-relative plot of the flight level pressure (not shown) indicates that the plane descended from 700 hPa to 850 hPa during this outbound leg.

2.7 Extended Flight Level Data Set

The resulting *Extended Flight Level Data Set* (or *FLIGHT+*) covers nearly all TCs that have been flown in the North Atlantic, Eastern Pacific, Central Pacific, and Western Pacific basins from 1997-2013. The data set format has been designed to enable a wide range of industry and research uses. The data set will

[4]The unbinned data extend out to larger radius because the binned data are subject to leg termination criteria if the pressure varies by more than 10 hPa from the average pressure of the first 25 km of the leg.

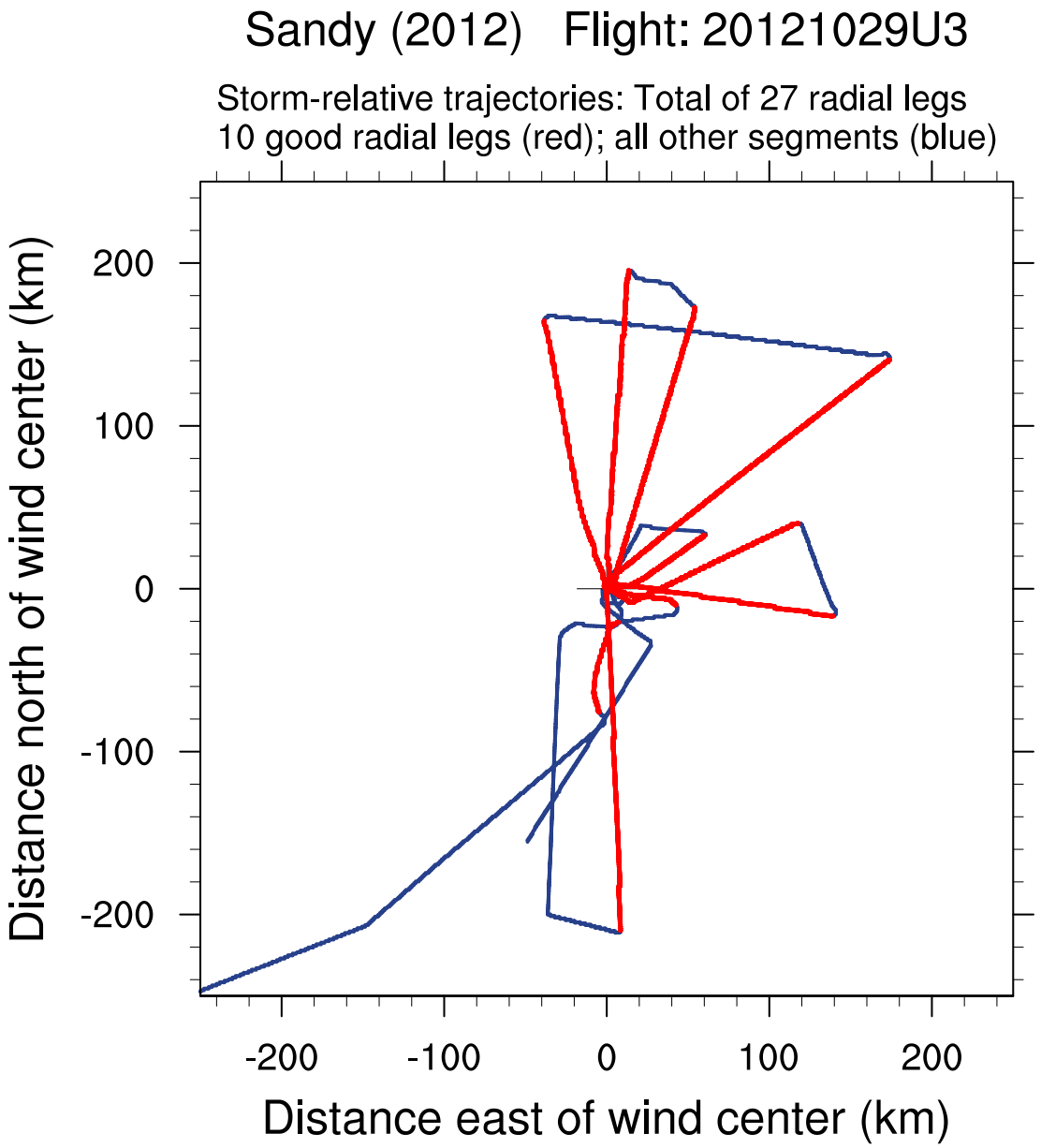

Figure 11: Flight trajectories in storm-relative coordinates for the final flight before Hurricane Sandy made landfall in New Jersey. Portions of the flight trajectory identified as 'good' radial legs are shown in red. All other flight portions are shown in blue.

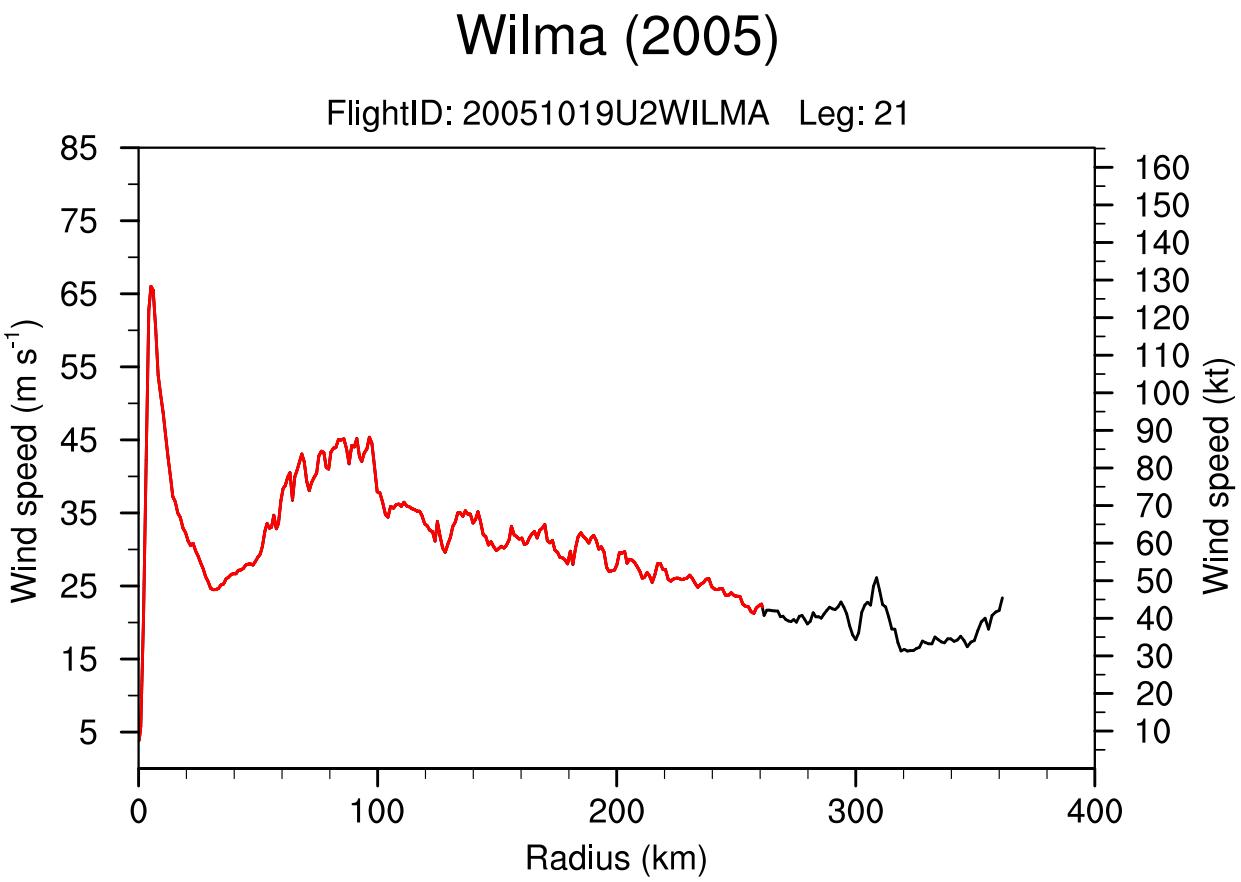

Figure 12: Comparison between the binned (red curve) and unbinned (black curve) data for a radial leg in Hurricane Wilma on 19 October 2005. In order to ensure that only data on a quasi-constant flight pressure surface are shown, the binned data are terminated if the flight level pressure varies more than 10 hPa more than the average flight level pressure near the storm center. Thus, the binned data end at about 260 km radius while the unbinned data continue to larger radius. The very close correspondence between the binned and unbinned data show that the linear interpolation does not appreciably change the wind speed values.

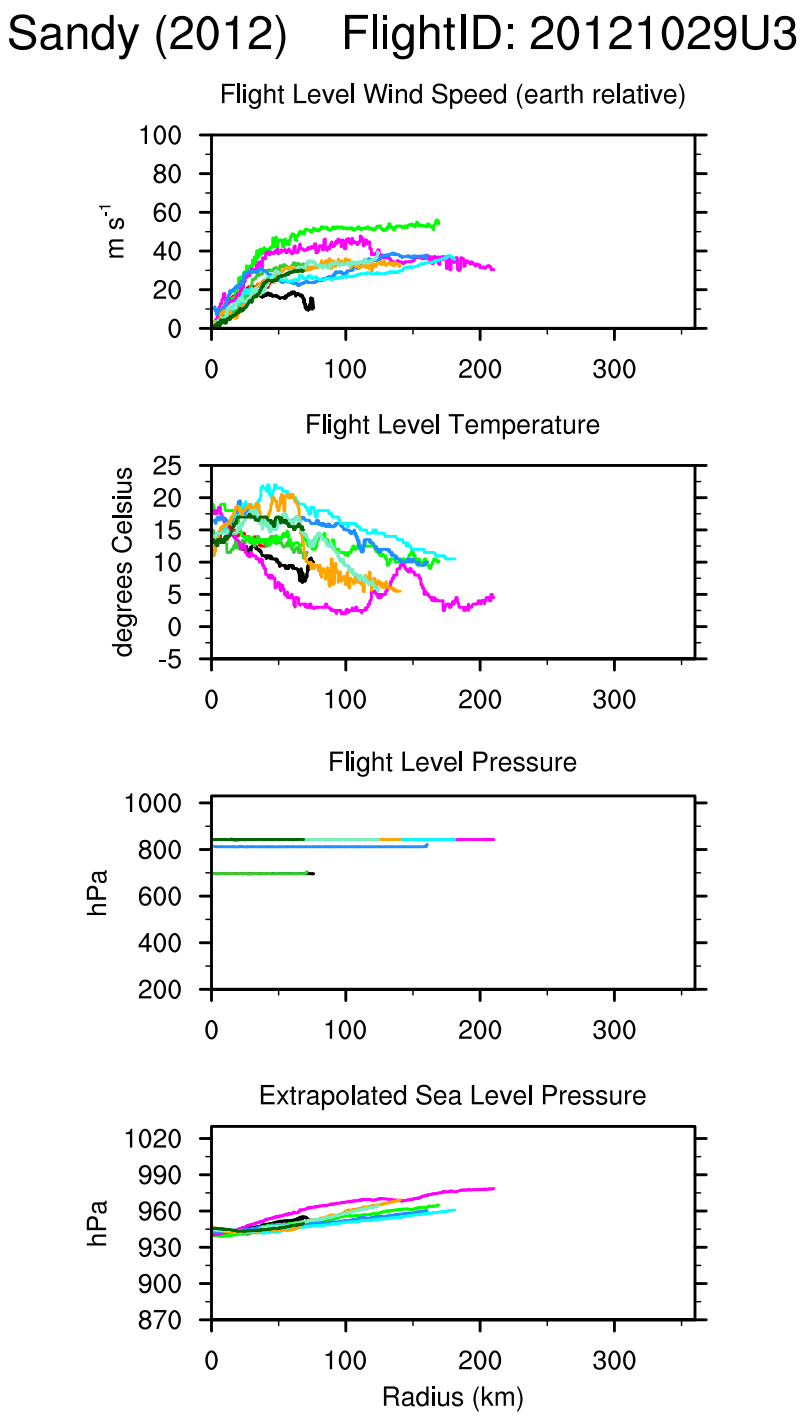

Figure 13: 'Good' radial legs for the final flight before Hurricane Sandy made landfall in New Jersey. Panels from top to bottom: (a) flight level wind speed, (b) flight level temperature, (c) flight level pressure, and (d) extrapolated sea level pressure. Each radial leg is represented using the same color in each panel.

be publicly released to the research community in 2015.[5] Please check the FLIGHT+ page on the Tropical Cyclone Data Project (TCDP) web site for updates on the data set release schedule: http://verif.rap.ucar.edu/tcdata/flight/. Detailed graphical plots of the flight level data for each storm are already available at: http://verif.rap.ucar.edu/tcdata/flight/applications/. These plots include the earth-relative data, graphical summaries of the storm-relative parsing, and plots of the radial legs. The data set files include all of the typical navigational and meteorological parameters that are commonly available in both the AFRES and NOAA source data files.

3 APPLICATION OF THE SYNTHETIC PROFILES TECHNIQUE

With the hard work of processing the aircraft data finished, the trajectories flown in the real storm can now be used to define synthetic trajectories in the model space. This section describes the implementation of a module to construct synthetic profiles from fields of the operational Hurricane WRF (HWRF) model, although the technique can be applied to any numerical weather prediction output (e.g., global models, other regional hurricane models). This section describes the basic approach to applying the synthetic profiles technique, how the model-observation matching is accomplished, the methodology used to sample the model fields to create the synthetic profiles, and further details about the module code set.

3.1 Basic Approach and Philosophy Guiding the Application of Synthetic Profiles

The basic approach used to develop this module has been inspired by the work of Uhlhorn and Nolan (2012), who used synthetic profiles to study some theoretical aspects of the likelihood that an observing system will sample the highest wind speed as a storm translates past. Uhlhorn and Nolan were able to run a WRF-based nature simulation at extremely high temporal resolution (e.g., 10 s) for part of their idealized study, with hourly snapshots outside of the intensive study period. However, since the current implementation seeks to apply the technique to operational model output, we must work within the constraints of what is available in the target model, which is the operational HWRF. In real-time HWRF runs, the output is stored every three hours. Each of these output files represents an instantaneous snapshot (or 'time slice') for certain fields (the files also contain fields of accumulated quantities such as precipitation). While HWRF could be rerun at very high temporal frequency, it is not practicable to store such large volumes of data. As it turns out, it is not necessary either. If the simplifying assumption can be made that the movement of small-scale elements in the flow of the hurricane can be neglected during the sampling period, we can then sample the given model time slice instantaneously as if the plane were able to fly the entire radial leg in one instant. This assumption should be valid so long as the period of time from the actual radial leg is relatively small, and the small scale features rotating around the storm are of relatively small amplitude and/or do not have strong gradients in the parameter of interest. When the plane is flying in the actual storm, it is typically flying at 115 m s^{-1}, which means that it flies a standard 200 km radial leg in approximately 30 min. While elements can certainly rotate a substantial distance around the eyewall of a hurricane in that amount of time, the effect of such features on the data gathered in the real storm can be treated as noise if the amplitude of variations is low enough. As will be shown in the results, the variability in the actual radial legs is fairly small, which suggests that the amplitude of these features is normally quite small. Thus, our assumption is valid and we are justified in sampling the model time slice instantaneously.[6]

[5] The dataset can be made available to friendly collaborators for non-commercial research purposes in advance of the public release.

[6] As a side note, Uhlhorn and Nolan (2012) used four-dimensional interpolation (where the fourth dimension is time) during the part of their study in which the model output was stored at hourly intervals. The effect of interpolating in time between hourly slices will tend to smooth out such finescale features, preserving only the gross features of the vortex. So in order to actually sample the small-scale variability, one must sample the model at very high temporal frequency which is not practical unless the

3.2 Model-Observation Matching

In order to construct synthetic profiles, it is first necessary to determine which model time slices match available observations. In the current version of the module, this matching is done at the storm-level, as follows. First, a list is created of all of available model cycles for this storm. Then the module loops over each model time slice for each cycle, starting at the analysis time ($t = 0$) and checking each subsequent file at 3-hourly intervals to the end of that particular model simulation. The valid time for each time slice is constructed and then checked against all available observed radial legs for the storm. Any observed radial legs whose mid-point time falls within ± 1.5 h of the valid time of the particular model time slice are considered a match, and are stored for later reference.[7]

3.3 Sampling Methodology for Creation of Synthetic Profiles

Once the list of all radial legs that match the available model time slices has been created, the program then loops through each time slice and reads the three-dimensional field of interest from the HWRF simulation (e.g., wind speed, temperature, etc.). These fields have already been post-processed into a regular lat/lon grid at 42 regular pressure levels with 25 hPa spacing in the lower troposphere. The program also reads the hourly track file in the 'a-deck' format of the Automated Tropical Cyclone Forecast (ATCF) system (Miller et al. 1990; Sampson and Schrader 2000). This track file is generated by the HWRF post-processing using the GFDL vortex tracker (Tallapragada et al. 2014).[8] For purposes of visualization later on, the two-dimensional field at the closest model pressure level to the average pressure of the radial leg is stored for future reference.

Next, the storm-relative coordinates of the observed flight trajectory are translated to the earth-relative (lat/lon) coordinates centered on the model's simulated storm. These lat/lon coordinates then form the basis for the synthetic trajectory. The code samples along this trajectory point-by-point, first interpolating horizontally at the nearest pressure levels above and below the pressure of the trajectory, then interpolating vertically between the two horizontally-interpolated points.[9] The resulting synthetic radial leg wind speed data are then stored in arrays. Currently, the module only creates synthetic radial legs of the *earth-relative* flight level wind speed, however it will be relatively easy to add additional flight level parameters, as well as surface wind speed. It would also be relatively easy to compute storm-relative winds for comparison with the storm-relative wind in the real storm.

It is always possible that two or more aircraft may have flown simultaneously in the storm (and at multiple levels), so the module has been designed to handle this multiple-aircraft scenario.[10] This leads to some rather complex data structures. When all of the matching time slices have been processed thusly, the synthetic radial legs are written out to a NetCDF file along with the associated metadata and the stored

sampling is done on-line while the model runs. Doing the sampling online would preclude real-time applications however, since the exact flight patterns cannot be known with certainty in advance.

[7] Note: the threshold of 1.5 h has been chosen to ensure that each available radial leg will get matched if a model time slice exists for that time window, while also preventing any radial leg from being matched with more than one model time slice and hence being double counted. If this module is used for verification purposes in the future, it would be important to prevent double-counting, so setting the match window at the greatest possible time while avoiding double counting seems to be the best choice.

[8] The program also has the capability to read the High Frequency Tropical Cyclone Forecast (HTCF) format, however since that data type only includes the lat/lon pairs of the innermost mesh rather than the simulated storm center, it is not very useful for synthetic profiles.

[9] Dennis Shea recommended this two-step interpolation method, rather than developing a new routine for three-dimensional interpolation. Because NCL already has existing routines to do this type of horizontal and vertical interpolation, it was easy to implement this two-step interpolation method. The accuracy of this method should be superior to, or comparable to the result from basic three-dimensional interpolation.

[10] There is no actual requirement that the observing platform be aircraft – the technique could be applied to other types of remotely sensed data as well.

model fields nearest to the average pressure level of each radial leg.

3.4 Further Details about the Module Code Set

The module code set has been prototyped in NCAR Command Language (NCL 2014), a versatile high-level interpreted programming language. At the top level, the code set includes a driver script (written in NCL) that is capable of constructing a list of desired jobs and then submitting batch queue scripts in a supercomputing environment. The top-level driver can also run individual jobs in sequence on a workstation. Once the batch queue script for a job has been constructed and submitted, an intermediary script (written in `bash`) is called to initialize the various log files and check that key paths are present. This intermediary script then invokes the appropriate run-level program (written in NCL). A run-level NCL program exists for each of the seven steps that are necessary to process the flight level data and then create and visualize the synthetic radial legs. The steps involved in creating synthetic radial legs are summarized as follows:

- Step 1: Standardization of earth-relative aircraft data (output written to an internal L1 data file for each storm),
- Step 2: Generation of plots of the earth-relative data for QC,
- Step 3: Parsing of the observed aircraft data into 'good' radial legs (output written to an internal L2 data file for each storm),
- Step 4: Translation of the aircraft data into storm-relative coordinates and binning of radial leg data (output written to an L3 data file for each storm),
- Step 5: Visualization of the aircraft radial leg data,
- Step 6: Find matching model time slices that correspond to available observed radial legs and then sample the model space to derive synthetic radial legs,
- Step 7: Generation of plots comparing the flight trajectories in the real storm to those in the model storm and comparing the resulting synthetic radial legs.

In order to expedite generation of the entire FLIGHT+ data set, steps 1-4 were run on the Yellowstone Supercomputer CISL (2014), while steps 6 and 7 were run on a local workstation.[11]

4 RESULTS

The synthetic profiles module has been tested on a set of fourteen retrospective simulations for Hurricane Sandy (2012) that were run by the National Centers for Environmental Prediction Environmental Modeling Center (NCEP/EMC) using the T14C test configuration of HWRF.[12] Only the 00Z and 12Z model cycles for Sandy have been used in this test, mainly due to hard disk storage space considerations. The model cycles start with the 00Z on 23 October and end with the 12Z cycle on 29 October. There are two dimensions in which one can browse the resulting output. One can hold the model cycle constant, varying the lead time to see how the simulated vs. real structures evolved for that one model cycle, or one can fix the verifying period and compare how different model cycles simulated the storm for that particular time period. We will show examples from both of these output dimensions.

[11] All of the steps are of a small enough computational size, however, that they can be run on a heavy-duty workstation if necessary.

[12] The T14C configuration is similar to the configuration of HWRF that is being used for real-time operational runs during the 2014 season.

4.1 Results for a given model cycle, varying forecast lead time

Figure 14 shows the first available model/observations match, which is for the model cycle analyzed at 00Z on 23 October. The first model time slice that matched available radial leg(s) was the 12-h forecast, valid at 12Z on 23 October. Figure 15 shows the comparison between the real storm and the HWRF-simulated storm for each of the radial legs (magenta curves) shown in Figure 14. At this time, the real storm was still quite weak and disorganized, while HWRF shows a more organized and intense storm with a pronounced wind maximum. While one could qualitatively infer the conclusions of the previous sentence through careful thought, taking into account the analyzed intensity of the real storm and comparing this with HWRF, the comparison between the synthetic radial leg wind speed and that of the real storm nicely illustrate the radial structure and dramatic difference between the real and simulated storms. While HWRF has a radius of maximum winds (RMW) of approximately 60 km, the real storm has a possible inner RMW of less than 10 km in one radial leg, and an outer RMW of at least 200 km. Note that the actual radial legs have not had any smoothing applied yet, but nevertheless, the HWRF wind structure is also much smoother than that of the real storm.

Moving to a later lead time, even more dramatic differences can be seen between the real and simulated storms. Figure 16 shows the radial leg comparisons for the same model cycle, but now at forecast hour 27. For this time slice, there were four matching radial legs, and these legs provide good azimuthal coverage of the storm. The HWRF-simulated storm has rapidly intensified in the intervening 15 h, with radial leg maxima of $50-55\,\mathrm{m\,s^{-1}}$ and RMW of $45-60$ km. Meanwhile, the real storm had also intensified, but not nearly as much, with radial maxima of $15-30\,\mathrm{m\,s^{-1}}$ and RMW ranging from $65-120$ km.

Figure 17 shows the radial leg comparisons for the 51-h forecast from that same model cycle. By this time, the real Sandy was a hurricane and displayed a mature TC structure with peaked inner core wind maxima. For the radial legs shown in the lower two panels, the HWRF-simulated storm displayed a qualitatively similar radial wind structure, however for the upper panels, very large differences can be seen. Indeed, the HWRF-simulated radial maxima are almost completely out of phase with the wind maxima in the real storm. Figure 18 shows the map-view of the trajectories plotted atop the model field; this shows that the simulated storm had a strong wavenumber-1 asymmetry with a quasi-elliptical eye feature. The real radial wind structure hints at a similar asymmetry in the real storm, but not to the degree of the simulated storm. This may be an example where the HWRF model generated some sort of eyewall or inner core instability (e.g., algebraic instability, Nolan and Montgomery 2000) whose magnitude was much stronger than the instability in the real storm.

The final match from the model cycle initialized at 00Z on 23 October 2012 comes at a forecast lead time of 120-h. Figure 19 shows the comparison between the real and synthetic trajectories at this time. This plot illustrates nicely the capability of the synthetic profiles technique to accurately sample the simulated storm even when the underlying model run has very large track error. Here the simulated storm has incorrectly turned right, while the actual storm is moving about the apex of a curve that eventually took it back toward land.

4.2 Results for a given verifying time point, varying model cycle

Now we turn our attention to the model cycles initialized closer to landfall. We focus on the verifying period of 18Z on October 29, which was just 6 h prior to landfall in southern New Jersey. Figure 20 shows the 42-h forecast that corresponds to the verifying target time. Likewise, Fig. 21 shows a 30-h forecast verifying at the same time, Fig. 22 shows an 18-h forecast verifying at that time, and Fig. 23 shows the 6-h forecast verifying at that time. In the first plot of this series (Fig. 20), the simulated storm is approximately 300 km from the actual storm and is extremely large, encompassing nearly the entire flight pattern that was flown. The simulated storm has two wind maxima: a more classical tropical inner core wind maximum

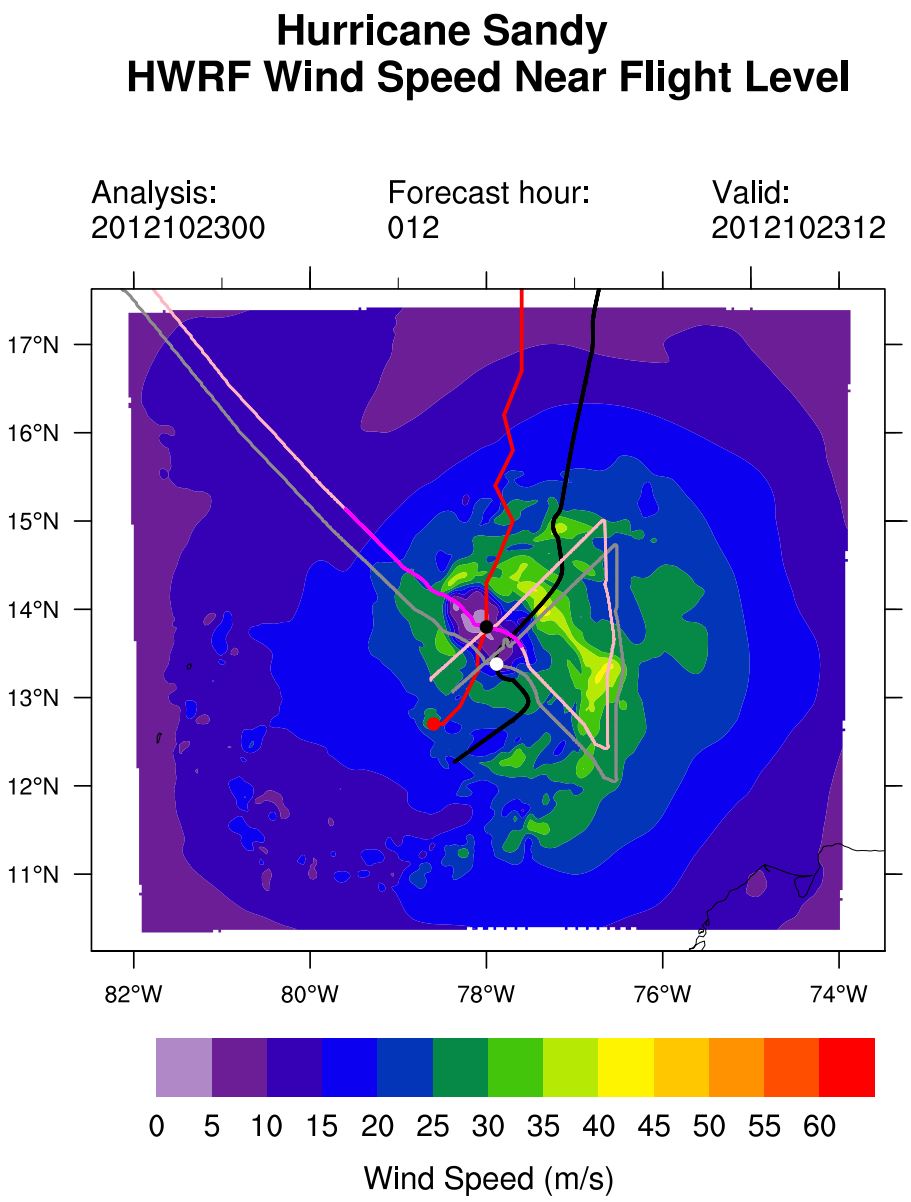

Figure 14: Comparison between the actual flight trajectory in the real Tropical Storm Sandy (grey curves) and the simulated trajectory that has been navigated onto the center of the HWRF-simulated Sandy (pink curves) for the 12-h forecast from the model cycle initialized at 00Z on 23 October 2012. The portions of the trajectory that correspond to the synthetic radial legs are also shown (magenta curves). For reference, the plot also displays the wind center track of the actual storm (black curve), the corresponding track of the HWRF-simulated storm (red curve), the position of the real storm at the analysis time (white dot), the position of the simulated storm at the analysis time (red dot), the position of the real storm at the time slice valid time (white dot), and the position of the simulated storm at the time slice valid time (black dot). The model's simulated wind speed is shown (color contours) at the pressure level nearest that of the average pressure of the first radial leg. While only radial legs whose midpoint times fell within ± 1.5 h of the model time slice are shown, the full flight trajectories are shown for a time window of ± 2 h to completely encompass any radial legs near the edge of the time window.

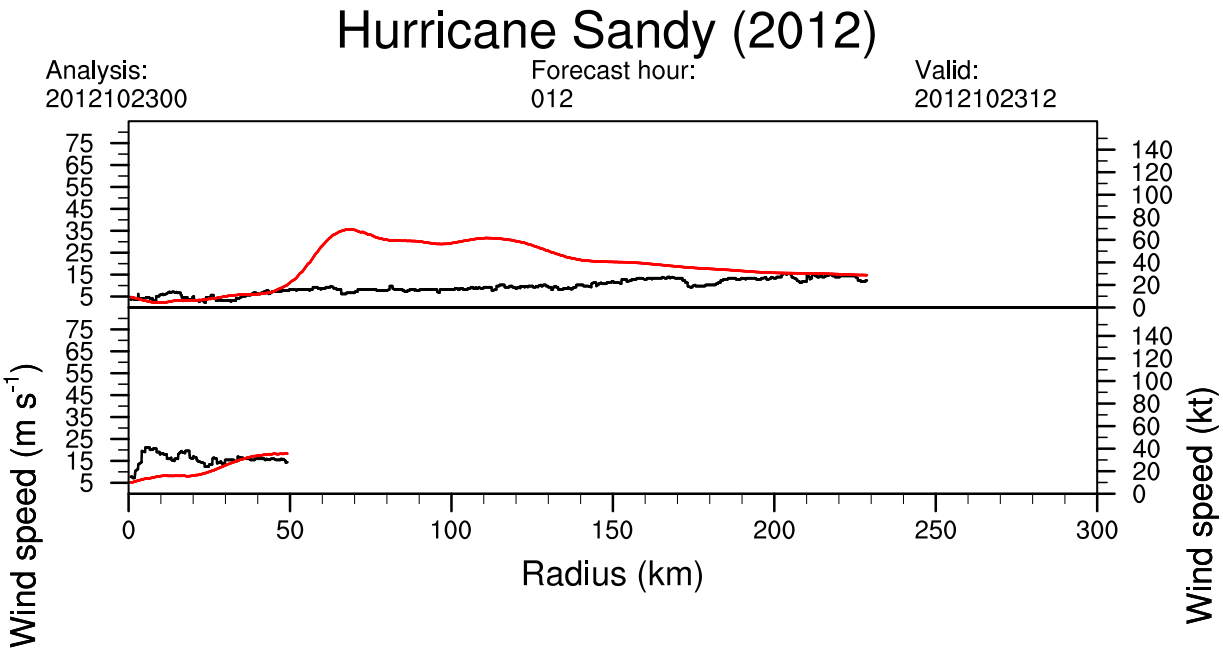

Figure 15: Comparison between the observed radial structure of flight level wind speed in the real storm (black curves) and the synthetically-derived flight level wind speed in the HWRF-simulated storm for each of two radial legs that fell within the match window for the 12-h forecast from the model cycle initialized at 00Z on 23 October 2012.

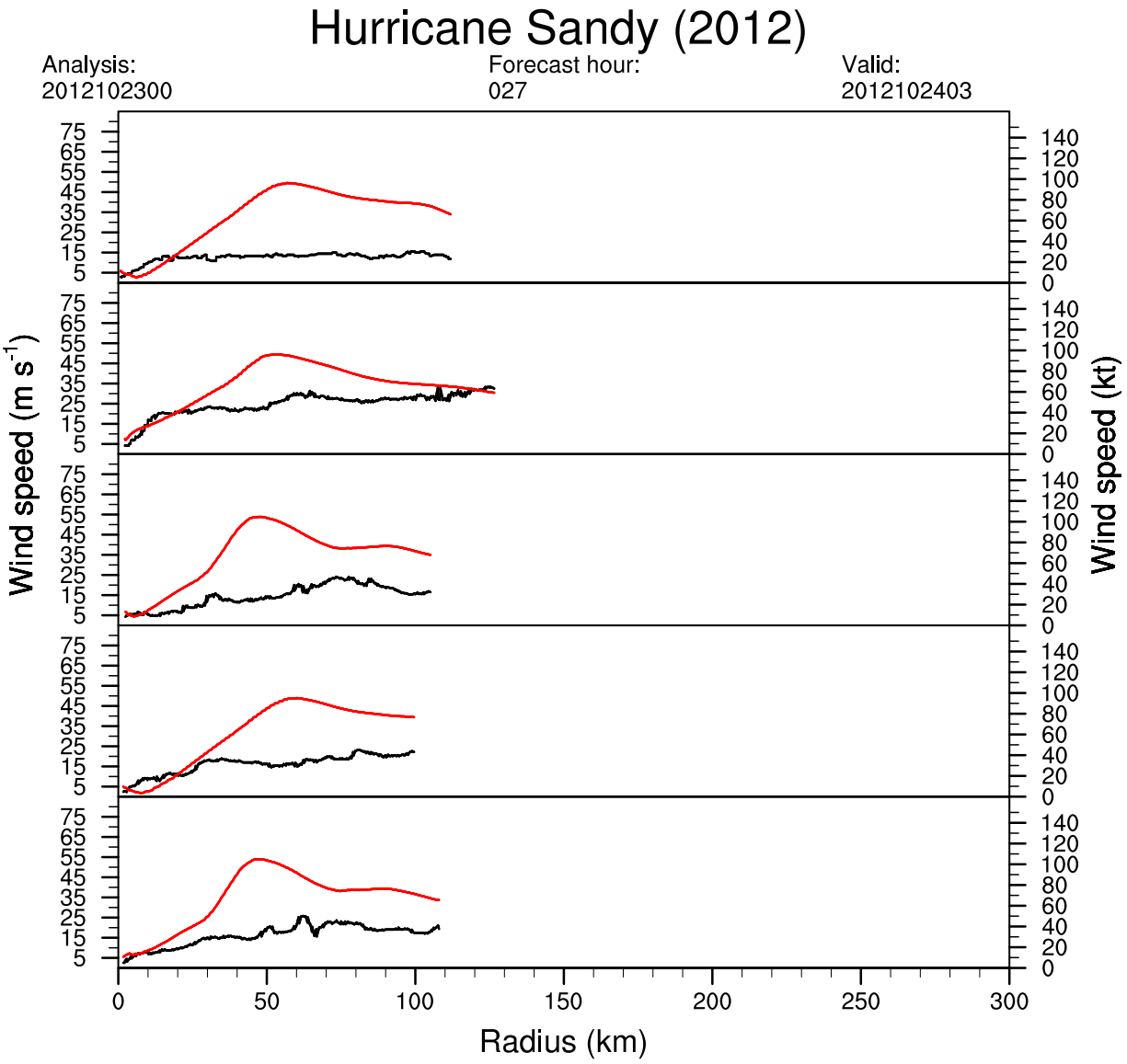

Figure 16: Comparison between the observed radial structure of flight level wind speed in the real storm (black curves) and the synthetically-derived flight level wind speed in the HWRF-simulated storm for each of two radial legs that fell within the match window for the 27-h forecast from the model cycle initialized at 00Z on 23 October 2012.

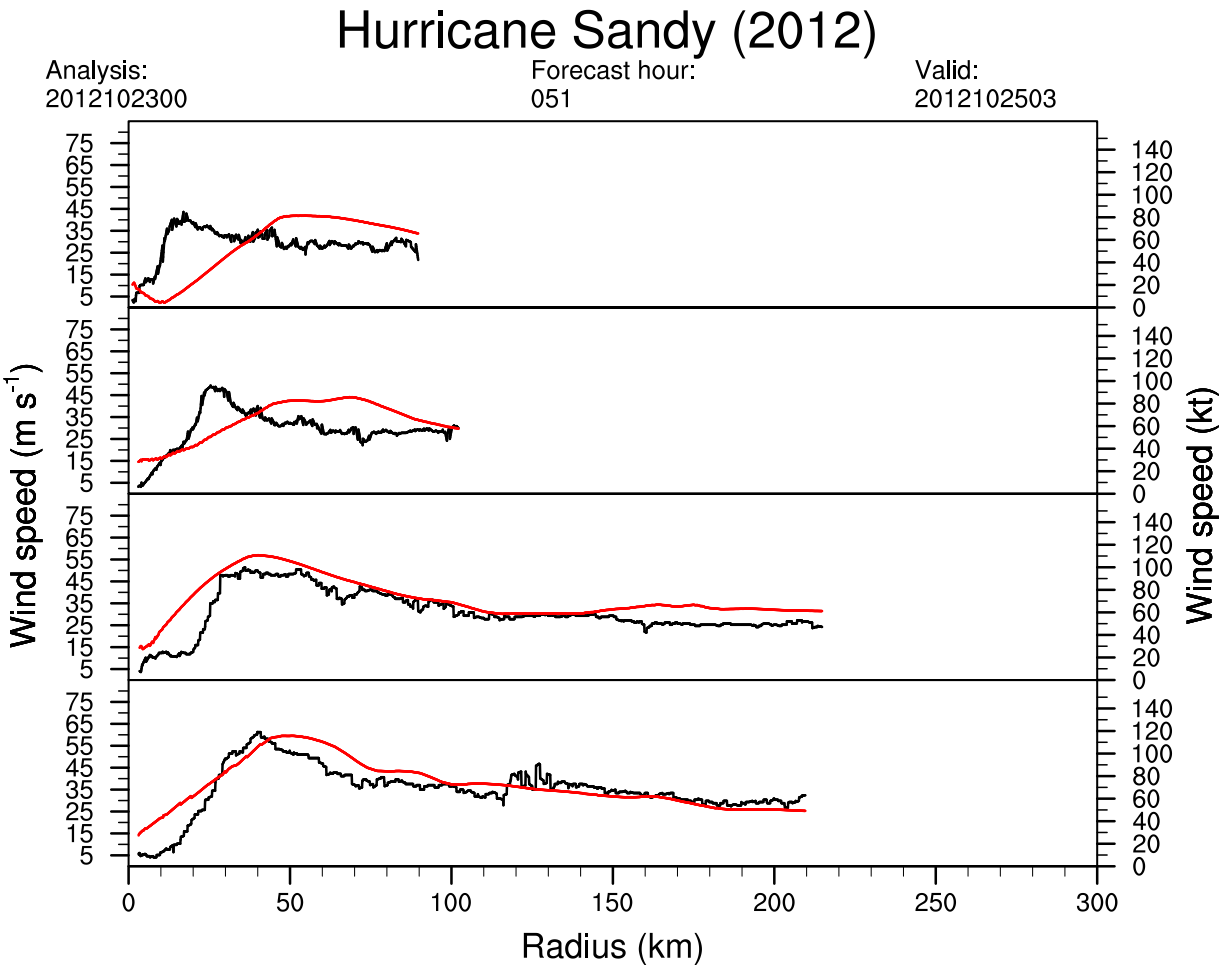

Figure 17: Comparison between the observed radial structure of flight level wind speed in the real storm (black curves) and the synthetically-derived flight level wind speed in the HWRF-simulated storm for each of two radial legs that fell within the match window for the 51-h forecast from the model cycle initialized at 00Z on 23 October 2012.

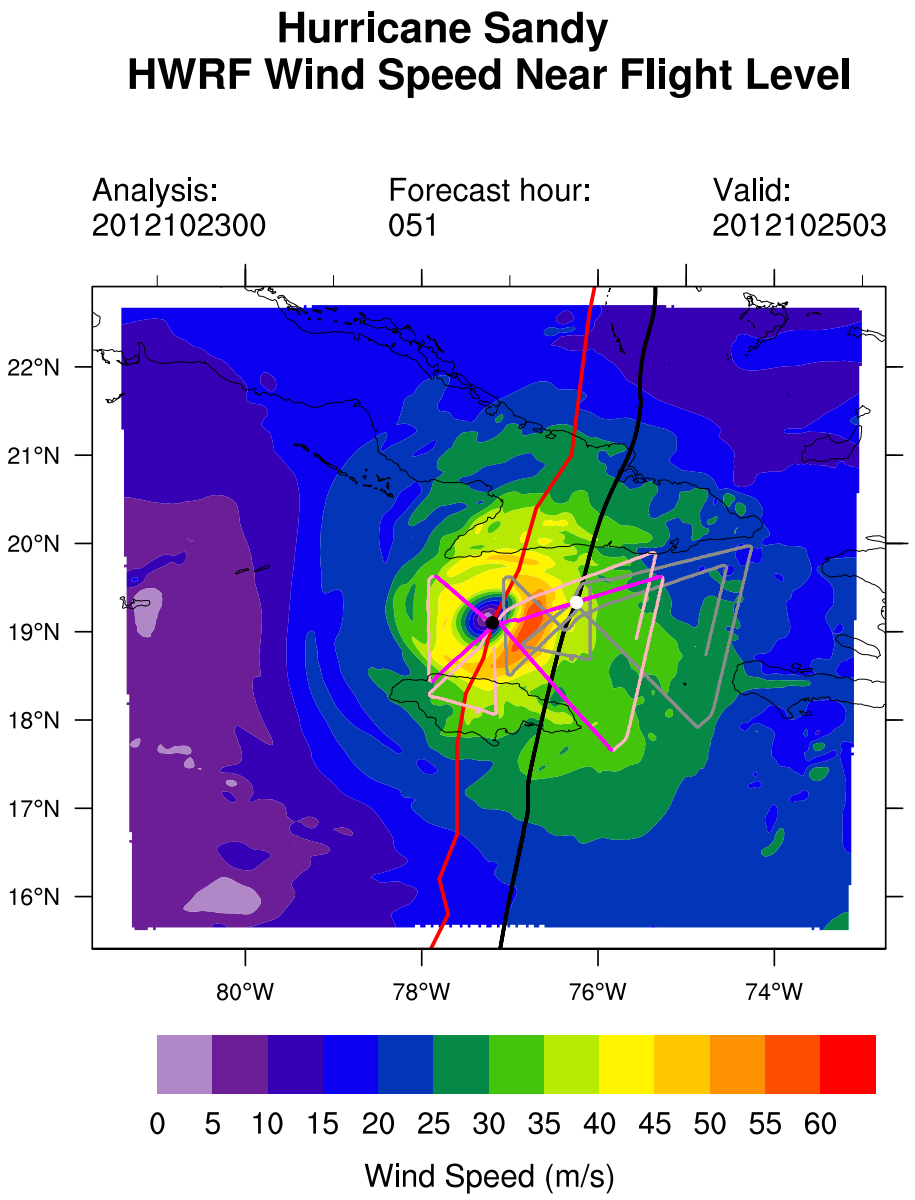

Figure 18: Plan view of synthetic trajectories for the 51-h forecast from the model cycle initialized at 00Z on 23 October 2012.

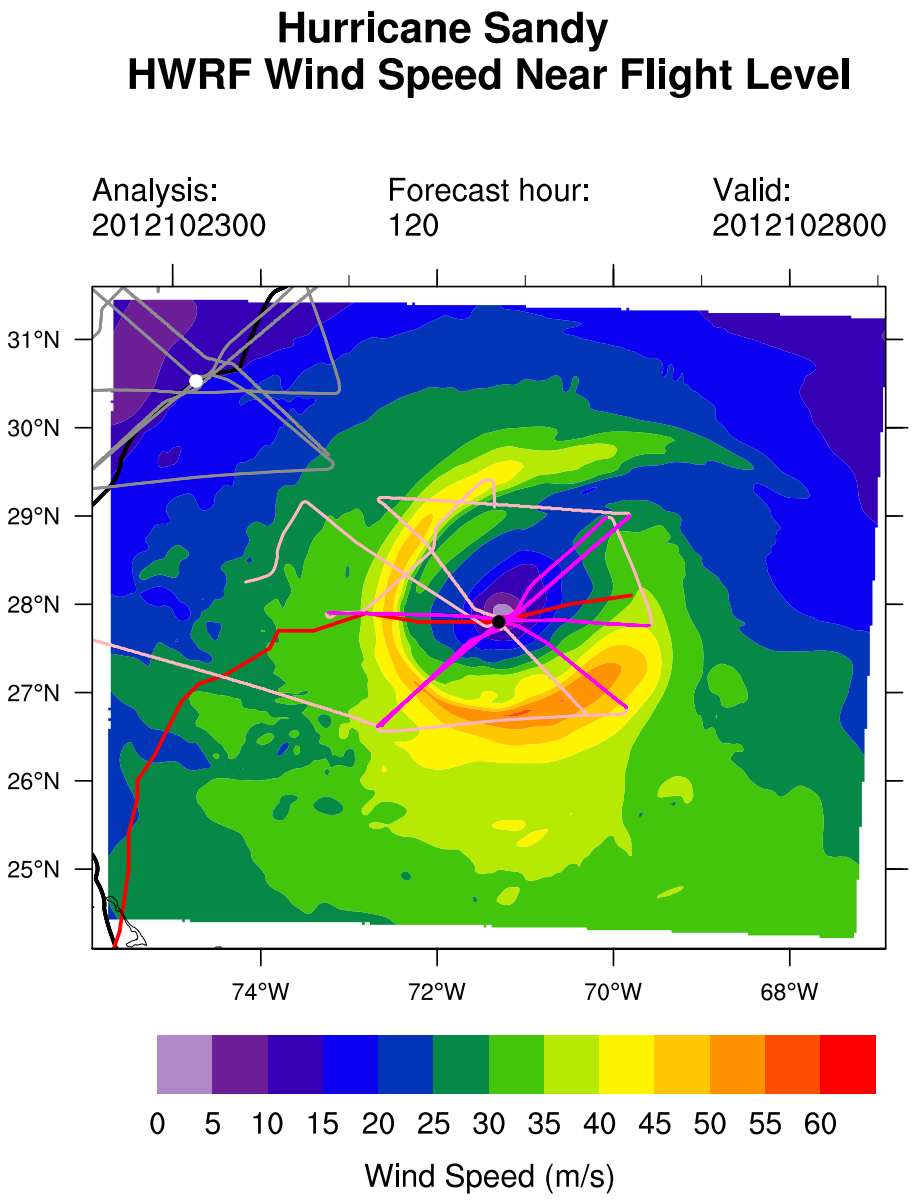

Figure 19: Plan view of synthetic trajectories for the 120-h forecast from the model cycle initialized at 00Z on 23 October 2012.

and a baroclinically-enhanced outer wind maximum. The outer wind maximum has a distinct oblong shape in the outer wind field – all of these features bear some resemblance to the actual storm at an earlier time period. The 30-h forecast (Fig. 21) is much closer to the actual storm position and still has an enormous outer wind band (perhaps slightly smaller than the 42-h forecast) as well as an inner core maximum. The orientation and degree of ellipticity of the outer wind band have changed compared to the forecast initialized 12 h earlier. Whereas the 42-h forecast had the strongest winds in the southeast quadrant, the 30-h forecast has winds of similar strength in both the southeast and northern quadrants. The inner wind maximum is also stronger in the 30-h forecast. The 18-h forecast (Fig. 22) is also near the actual storm position and has an even stronger inner wind maximum with less distinction from the outer wind band to the north, however the outer band is more oblong to the east and west. The 6-h forecast (Fig. 23) is actually farther from the location of the actual storm, does not have a distinct inner wind maximum, and has significantly stronger winds in the northern semicircle of the outer wind band. The radius of that outer wind band appears to be smaller than the forecasts at greater lead time. At this time, the real storm was transitioning to post-tropical and the inner wind core was rapidly losing definition. The 6-h forecast seems to be the best match to our understanding of Sandy's structure, at least from this qualitative examination of the sequence of forecasts of the wind field.

How well does this qualitative view hold up when using the more quantitative information offered by the synthetic radial legs? Figures 24-27 show the comparisons for the observed vs. synthetic radial legs for this set of four forecasts. Firstly, note that the two radial legs shown in the middle of the 4-panel plot are relatively well simulated by HWRF in all four forecasts. These legs correspond to the legs flown in the east and northeast quadrants of the storm. Because HWRF's inner core wind maxima in this run are oriented north-south, the northeast leg does not sample this maximum. The upper panel of each plot shows the radial leg flown through the southern part the storm. This segment passes through or near the simulated inner wind maxima in several of the earlier forecasts. In all but the final model cycle of this sequence, the HWRF-simulated synthetic leg is between 5 and 20 $\mathrm{m\,s^{-1}}$ greater than that of the observed leg in the real storm. We can conclude that the earlier HWRF forecasts overdid the strength of the inner wind maximum, while the final HWRF forecast had a more accurate representation of this decaying feature. Finally, we turn our attention to the radial leg shown in the lower panel of each plot. This panel corresponds to the leg flown to the north of the storm. In the first two forecasts (at 42- and 30-h lead times), the synthetic radial legs have wind speeds that are between 10 and 20 $\mathrm{m\,s^{-1}}$ lower than the observed radial leg between radii of 40 and 140 km. The 18-h forecast is much closer to the observed, but is still too low by about 10 $\mathrm{m\,s^{-1}}$ between 80 and 130 km. The final forecast is somewhat worse than the 18-h forecast. We should note that in all four forecasts, this northern leg did not extend radially outward enough to capture the simulated RMW. Thus, we cannot make conclusions about whether HWRF correctly captured the magnitude of the maximum winds in this band.

5 CONCLUDING REMARKS

5.1 Summary

The aim of this work has been to develop a prototype module to implement the synthetic profiles technique for the HWRF model and then to test the module on a series of model runs from Hurricane Sandy. The goal has been to determine the potential efficacy and utility of the technique for purposes of verification and model diagnostics. A 34,000-line code set has been devised to handle all of the steps needed to process the flight level data into a form that supports use in synthetic profiles. The data are first standardized, then translated into storm-relative coordinates, parsed into radial legs, and then interpolated into a high resolution radial grid with 100-m grid spacing. A significant amount of work has been undertaken to quality control the data. This work involved both formatting corrections to the source data files to ensure that they are read

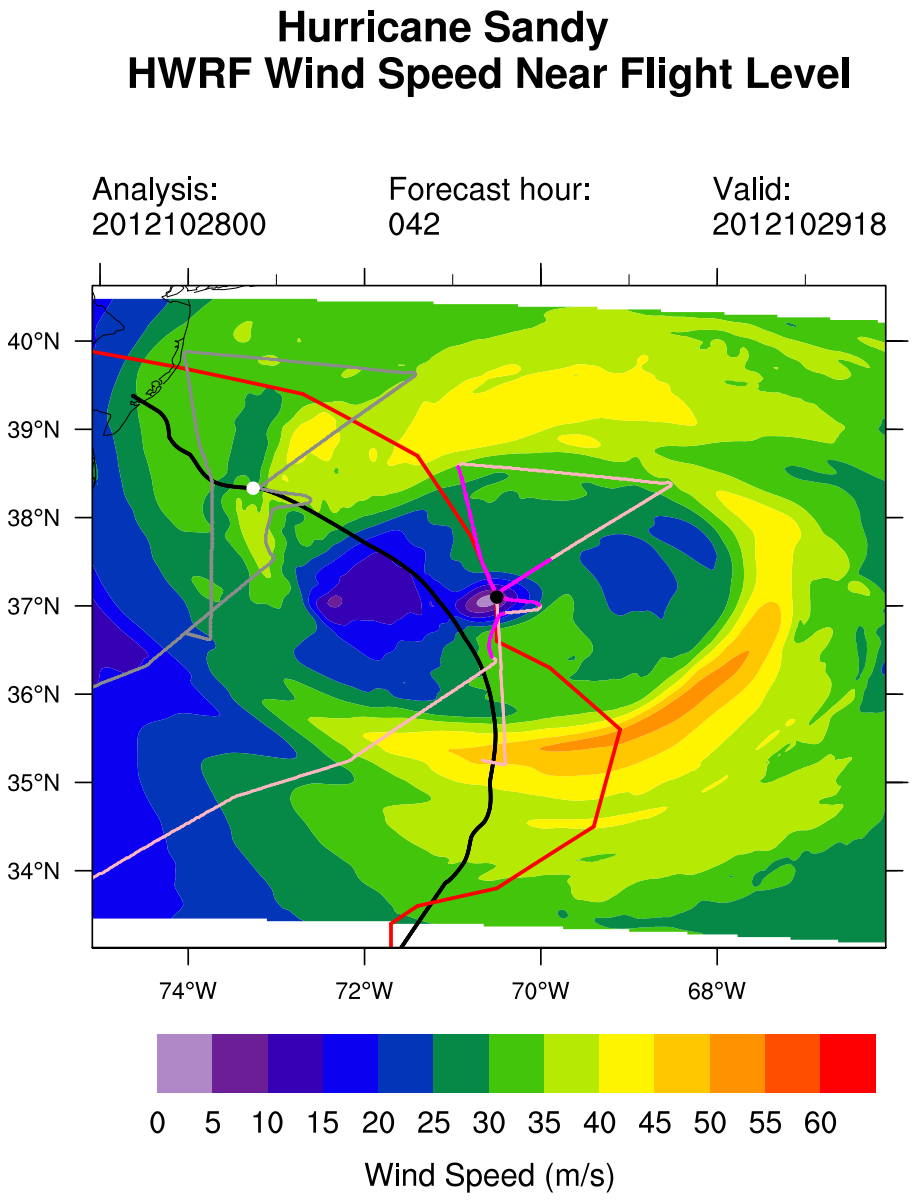

Figure 20: Plan view of synthetic trajectories for the 42-h forecast verifying at 18Z on 29 October 2012. This model cycle was initialized at 00Z on 28 October 2012.

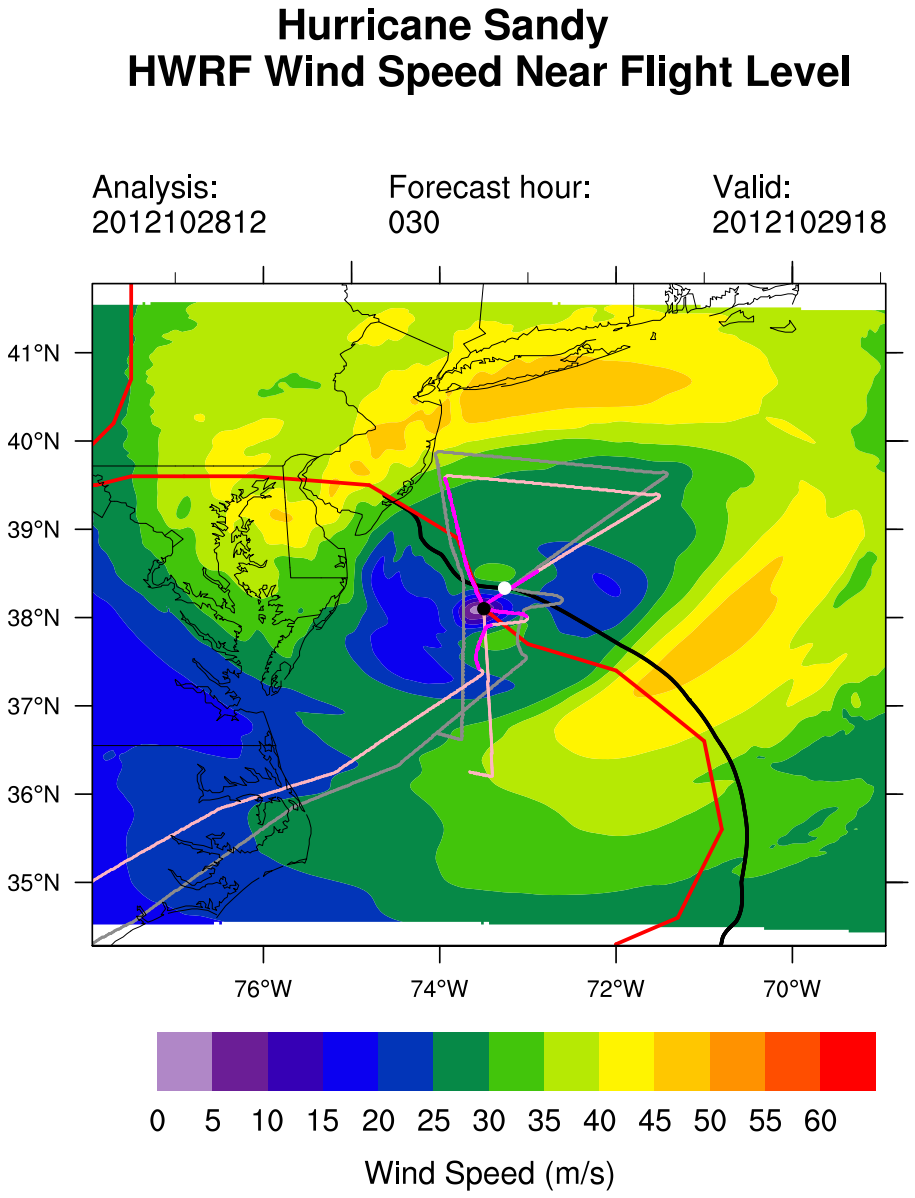

Figure 21: Plan view of synthetic trajectories for the 30-h forecast verifying at 18Z on 29 October 2012. This model cycle was initialized at 12Z on 28 October 2012.

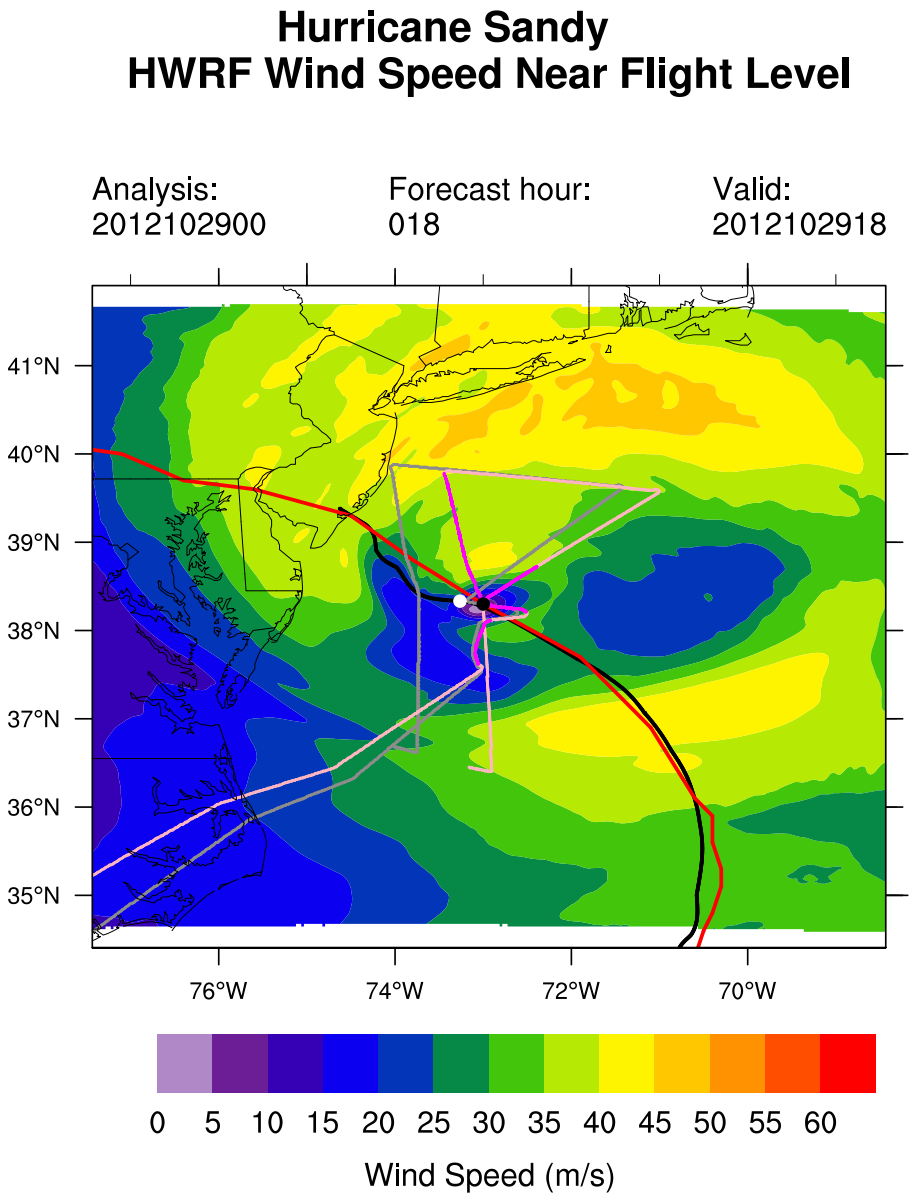

Figure 22: Plan view of synthetic trajectories for the 18-h forecast verifying at 18Z on 29 October 2012. This model cycle was initialized at 00Z on 29 October 2012.

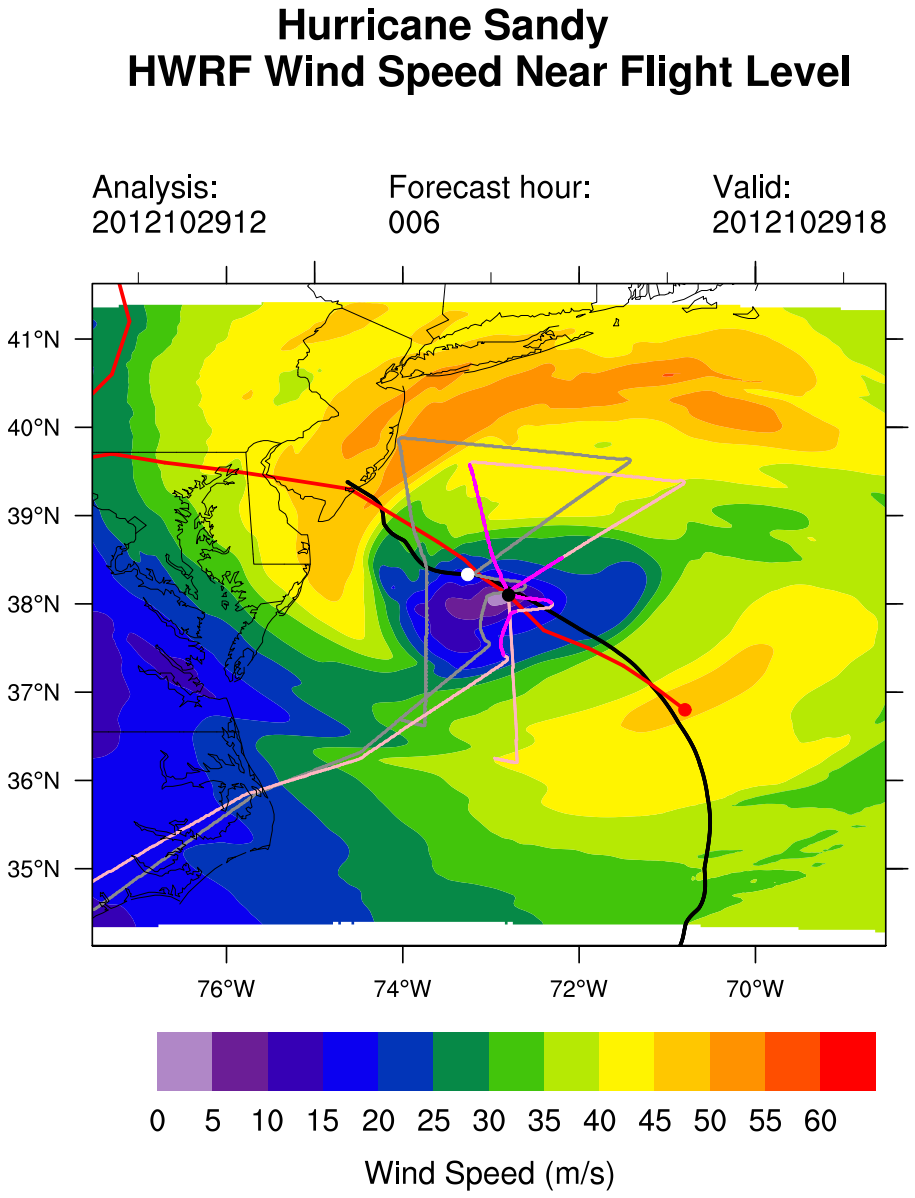

Figure 23: Plan view of synthetic trajectories for the 6-h forecast verifying at 18Z on 29 October 2012. This model cycle was initialized at 12Z on 29 October 2012.

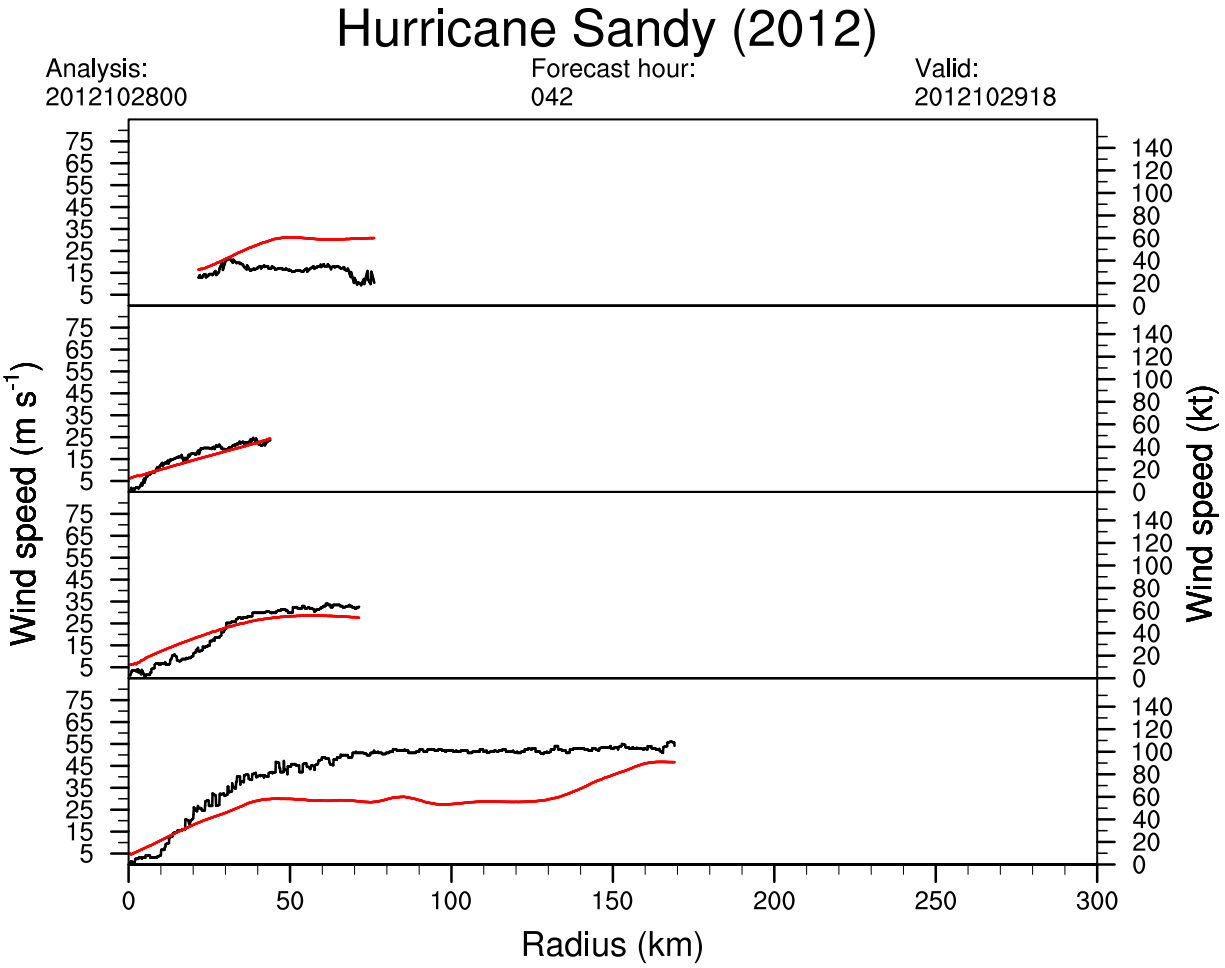

Figure 24: Comparison of synthetic and real wind structure for radial legs for the 42-h forecast verifying at 18Z on 29 October 2012. This model cycle was initialized at 00Z on 28 October 2012.

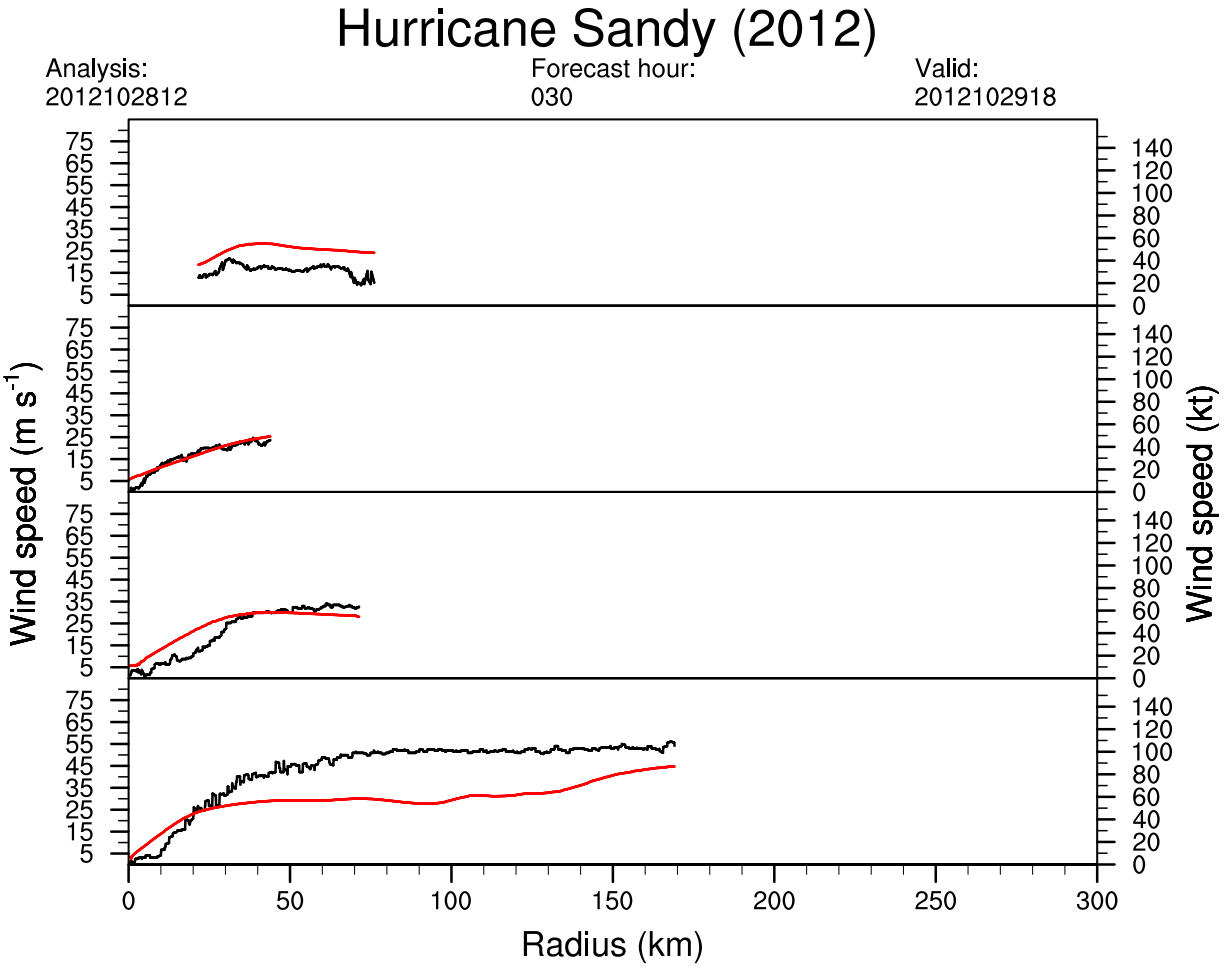

Figure 25: Comparison of synthetic and real wind structure for radial legs for the 30-h forecast verifying at 18Z on 29 October 2012. This model cycle was initialized at 12Z on 28 October 2012.

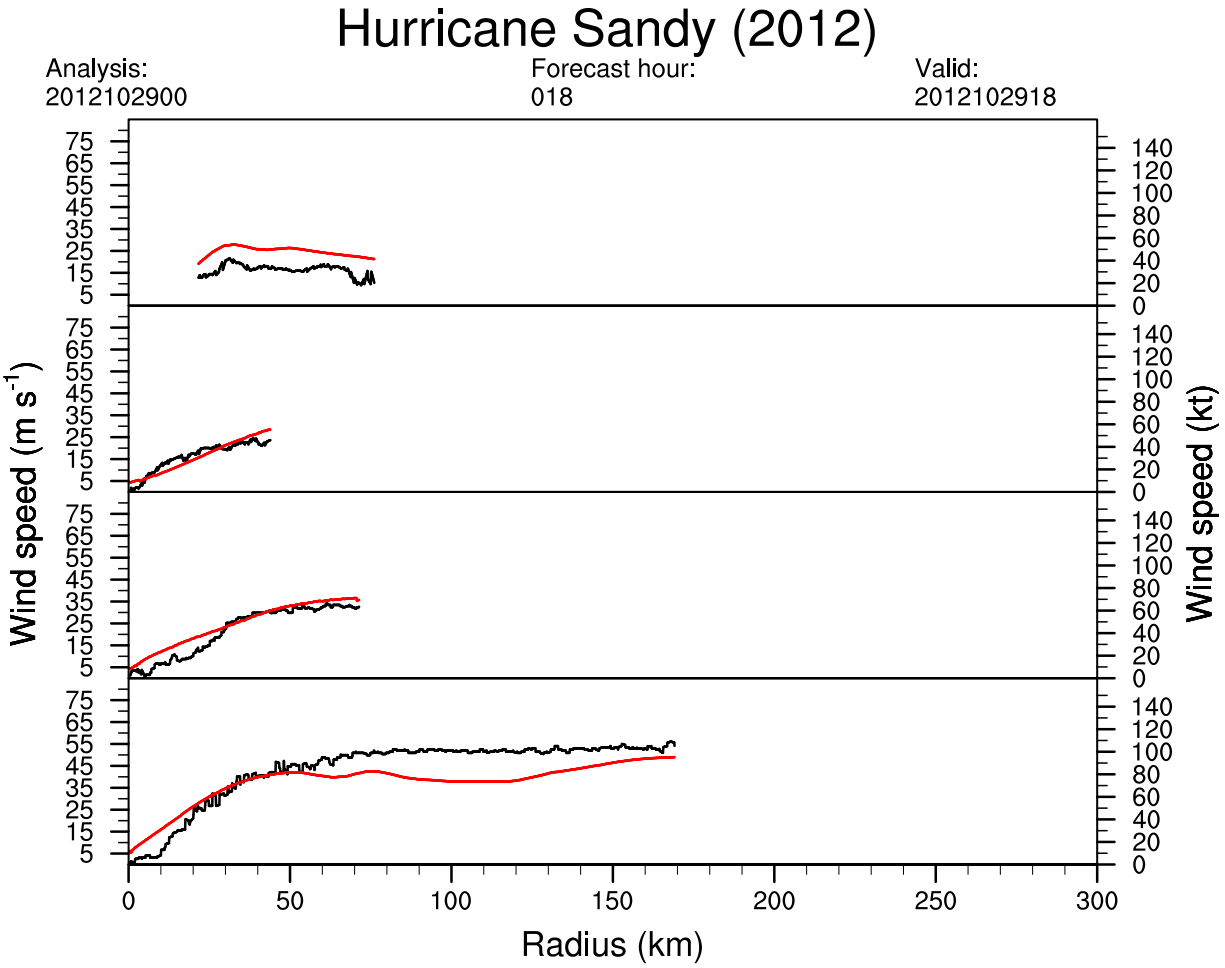

Figure 26: Comparison of synthetic and real wind structure for radial legs for the 18-h forecast verifying at 18Z on 29 October 2012. This model cycle was initialized at 00Z on 29 October 2012.

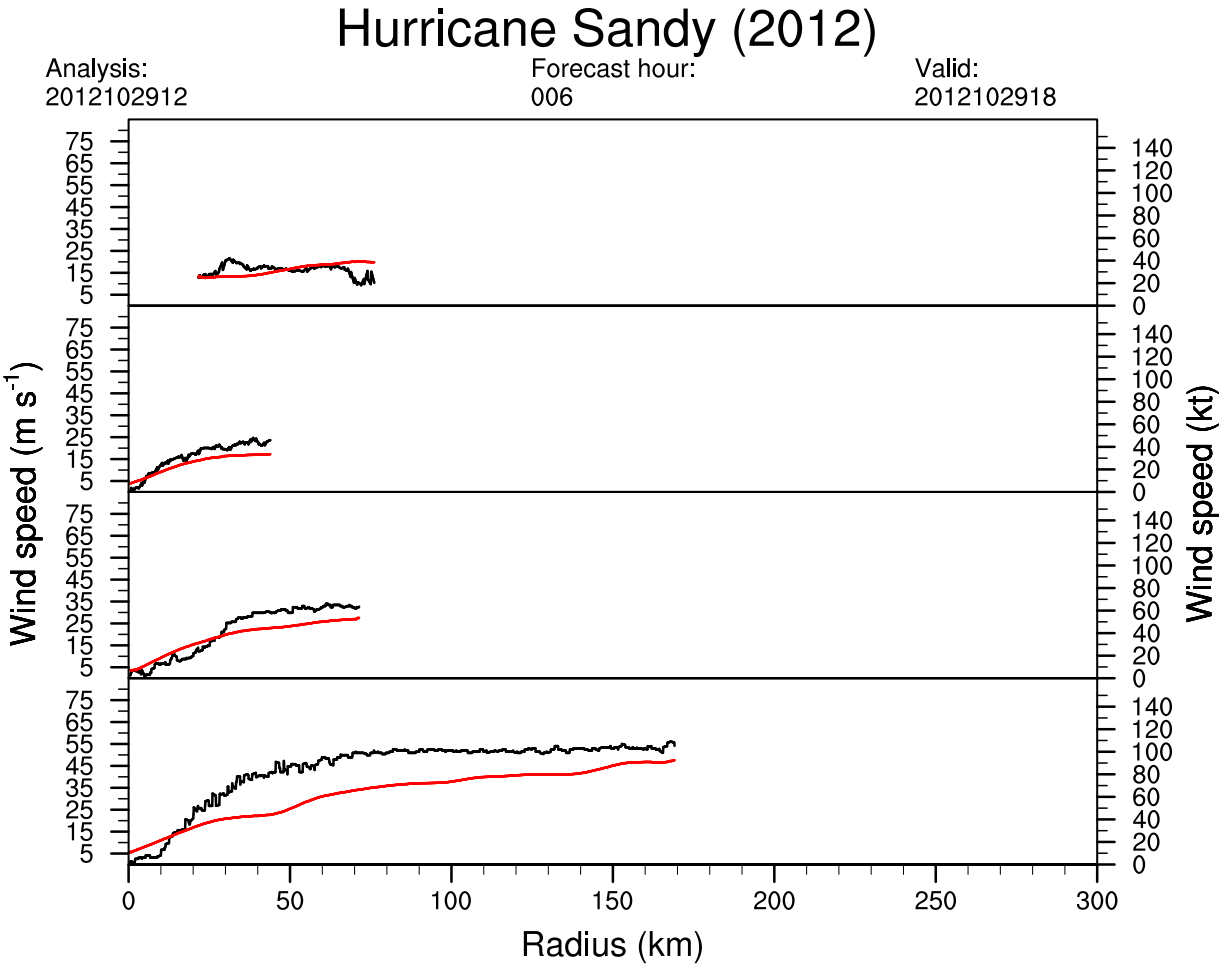

Figure 27: Comparison of synthetic and real wind structure for radial legs for the 6-h forecast verifying at 18Z on 29 October 2012. This model cycle was initialized at 12Z on 29 October 2012.

correctly, as well as extensive efforts to develop an algorithm to filter out poor quality SFMR surface wind speed data that result from wind retrievals over land, over shallow water, or when the plane was turning or rolling. The end result of these efforts is a high quality data Extended Flight Level Dataset (FLIGHT+) that has many potential uses beyond the current work.

The results from the test suite of Hurricane Sandy simulations show that the synthetic profiles technique is able to provide a wealth of high quality diagnostic information about the storm structure, considerably more so than is readily available merely by making eyeball comparisons. The suite of comparisons for just half of the model cycles for Hurricane Sandy resulted in over 350 model/observation matches. Some general conclusions can be drawn after perusing some of these comparisons:

- The technique is able to graphically illustrate the radial wind structure of the real and simulated storms in ways that are intuitive and readily understandable.
- The technique is able to uncover significant differences between the simulated and real storm structures, such as differences in the maximum wind speed, the RMW, and differences in the symmetry or asymmetry between radial legs.
- With some additional interpretation by the viewer, the technique can also illustrate differences in the representation of inner and outer wind maxima and other structural differences.
- HWRF initially intensified the storm too fast, leading to very large differences near the RMW in the early phases of Sandy.
- HWRF's representation of the baroclinic and tropical features of the storm generally improved with forecast lead time for the final set of forecasts prior to landfall. The final 6-h forecast had a better representation of the decaying inner wind maximum feature, as well as the overall size and strength of the outer wind band.
- HWRF's simulated storm had an outer wind band near landfall that may have been significantly larger than the actual storm. While it is difficult to conclude this, given that the radial legs in the final flight were too short, the wind structure in HWRF within the radial leg was still significantly weaker than the observed storm.
- HWRF's simulated radial wind structure is generally much smoother than the observed radial wind structure, with less variability.

On this last point, HWRF's wind structure is even smoother than one might expect given its 3 km inner grid mesh size. Normally, one might expect a NWP model to resolve features that are 6 to 8 times the size of its mesh size, however the wind maximum features in HWRF seem to be more on a scale that is 7-15 times the mesh size (or $21 - 45$ km). This albeit casual observation suggests that HWRF may have horizontal diffusion that is too high, or that some other factor in the model is leading to an incorrect cascade of turbulence.

5.2 Recommendations

Several recommendations can be made based on the experience gained in implementing the synthetic profiles in the prototype module and from the results of the Sandy test cases.

Firstly, if the synthetic profiles technique is to be used for operational verification, it may be necessary to modify the flight protocols based on storm size. This was graphically illustrated by the final examples from the Sandy test suite, in which the flight pattern fit almost entirely inside the outer wind band of the

model. In order to use the synthetic profiles technique to examine the full wind structure of the storm, it is essential that the radial legs flown extend radially outward of *both* the maximum wind in the real storm and the likely possible maximum wind in the modeled storm. This means that longer radial legs must be flown in larger storms. Extremely large storms such as Hurricane Sandy may require a two-plane mission in order to get enough data within a reasonable amount of time. When a dual-plane mission is not possible, flying 2 long passes through the storm would be preferable to flying 3 shorter passes.[13]

Another recommendation that can be made is that the latitude and longitude coordinates of the flight level data be stored with at least three digits of precision. When only two digits are used, the computation of incremental position change can be subject to floating point round-off error, which may lead to difficulty in parsing the radial legs. Due to this factor, it was necessary to use a running average of the 19-point centered difference of the position change instead of the instantaneous position change. Having three digits of precision may obviate the need for this measure.

5.3 Future Work

This current prototype module has only scratched the surface of what is possible with synthetic profiles. The PI hopes to find additional funding support to further elaborate on the capabilities of the module, as well as to test the sensitivity to a variety of factors in the technique. Briefly, the PI hopes to:

- Expand the module to generate synthetic radial legs for other flight level quantities such as temperature, dew point temperature, or diagnostics such as vorticity and θ_E.
- Expand the module to generate synthetic profiles of quantities remotely sensed by the SFMR instrument, including surface wind speed and surface rain rate.
- Add the capability to generate synthetic profiles of the extrapolated sea level pressure computed from flight level.
- Add the capability to subtract the motion of the simulated storm, thereby allowing comparison of the storm-relative wind speeds, and accurate computation of the azimuthal and radial wind components.
- Expand the module to run on a variety of NWP models.
- Add the capability to compute an azimuthal-mean profile from the available radial legs in order to examine and compare the symmetric structure.
- Examine the sensitivity to different spatial smoothing methods to determine the optimal amount to smooth the aircraft observations so as to match the spatial resolution of the model simulation.
- Examine the sensitivity of the technique to the stationarity assumption (that the synthetic radial leg can be taken as if the plane was able to instantaneously sample the storm).
- Examine the sensitivity to different methods of interpolation.
- Devise verification metrics to condense and summarize the comparison information.
- Devise other diagnostics, such as symmetry from the radial structure.
- Experiment with applying the Willoughby-Chelmow center finding technique to the *model* data, rather than relying on the tracker.

[13] This protocol may necessarily conflict with the tail-Doppler radar protocol, so it may not be possible to find a workable compromise in all cases.

The synthetic profiles technique can also be used to enable Observing System Simulation Experiments (OSSEs) in which the impact of observations on the model's analysis can be studied. The technique could also be readily applied to allow direct verification of wind analysis products such as H*WIND (DiNapoli et al. 2012) and the Multi-Platform Satellite Surface Wind Analysis (Knaff et al. 2011). The FLIGHT+ dataset may prove very useful for additional work in data assimilation, such as using storm-centered approaches (e.g., Navarro and Hakim 2014), or approaches that utilize the surface pressure field more heavily (e.g., Davidson et al. 2014). The PI plans to provide QC'd SFMR data to data assimilation experts at NCEP/EMC for further study to see if the higher quality data can lead to better use in inner core data assimilation.

Finally, in the future we hope to apply the synthetic profiles approach to the curving trajectories of dropsondes. As the resolution of regional and global hurricane models increases to ever finer scales, this approach may provide a more useful and direct way to examine the low-level vertical thermal and kinematic structures in simulated storms. We also hope to explore potential real-time applications that could result in improved "guidance-on-guidance" for intensity and structure prediction.

ACKNOWLEDGMENTS

An enormous debt is owed to the brave flight crews of the 53rd Weather Reconnaissance Squadron, NOAA's Aircraft Operation Center, and the Hurricane Research Division scientists who put themselves at risk each and every time they go out to collect these vital data. Without their dedication and diligence, this data set would not exist. I especially honor the crew members of the three planes who paid the ultimate price to collect these data.

I am extremely grateful to the NOAA Hurricane Research Division for provisioning all of the flight level data, which no doubt has been a very time consuming task. Without HRD's support, little progress would have been made. The wind center track files that are so crucial to this project were painstakingly constructed over many years by the late Ed Rahn, and more recently, by Neal Dorst. Neal Dorst in particular has done a tremendous job at supporting this project on the HRD side. Much thanks to Dr. Frank Marks for his support of this initiative. I also thank Neal Dorst, Barry Damiano, Sonia Otero, Richard Henning, Eric Dutton, and Jack Parrish for answering my many questions about the AOC and AFRES flight data formats and for helping to rescue 'lost' data for certain flights.

I owe a debt of gratitude to Mary Haley, David Brown, Wei Huang, Rick Brownrigg, Dennis Shea, and the entire NCAR Command Language (NCL) development team for their wonderful support and programming advice. They often went above and beyond the call of duty to assist in troubleshooting difficult issues that were encountered. Dennis Shea contributed a helpful suggestion about how to interpolate the model data. I thank Christopher Williams for his assistance in quality controlling the flight level data.

I acknowledge high-performance computing support from Yellowstone (ark:/85065/d7wd3xhc) provided by NCAR's Computational and Information Systems Laboratory, sponsored by the National Science Foundation.

I thank Vijay Tallapragada and Chanh Kieu at the National Centers for Environmental Prediction Environmental Modeling Center for providing the HWRF model data used in this work. I also thank Louisa Nance for providing helpful comments that improved an earlier version of this report.

The initial work on extending the flight level data set was supported by NASA/TCSP Grant NNG06GA54G and NSF Grants ATM-0332197 and ATM-0837932. The Risk Prediction Initiative (RPI2.0) provided substantial funding support to extend and modernize the flight level dataset. The Development Testbed Center Visitor Program (DTCVP) provided the main funding support to develop and implement the synthetic profiles technique. The DTC is funded by the National Oceanic and Atmospheric Administration, Air Force Weather Agency, and the National Center for Atmospheric Research. Funding for the DTC Visitor Program is also provided by the National Science Foundation.

References

Amante, C. and B. W. Eakins, 2009: ETOPO1 1 arc-minute global relief model: Procedures, data sources and analysis. NOAA Technical Memorandum NESDIS NGDC-24. National Geophysical Data Center, NOAA. http://dx.doi.org/10.7289/V5C8276M. [Accessed 03 June 2014.].

CISL, 2014: Computational and Information Systems Laboratory. Yellowstone: IBM iDataPlex System (Climate Simulation Laboratory). Boulder, Colorado: National Center for Atmospheric Research, http://n2t.net/ark:/85065/d7wd3xhc., http://n2t.net/ark:/85065/d7wd3xhc.

Davidson, N. E., et al., 2014: ACCESS-TC: Vortex specification, 4DVAR initialization, verification, and structure diagnostics. *Mon. Wea. Rev.*, **142**, 1265–1289, doi:10.1175/MWR-D-13-00062.1.

DiNapoli, S. M., M. A. Bourassa, and M. D. Powell, 2012: Uncertainty and intercalibration analysis of H*Wind. *J. Atmos. Ocean. Technol.*, **29**, 822–833, doi:10.1175/JTECH-D-11-00165.1.

Knaff, J. A., M. DeMaria, D. A. Molenar, C. R. Sampson, and M. G. Seybold, 2011: An automated, objective, multiple-satellite-platform tropical cyclone surface wind analysis. *J. Appl. Meteor. Climatol.*, **50**, 2149–2166, doi:10.1175/2011JAMC2673.1.

Miller, R. J., A. J. Schrader, C. R. Sampson, and T. L. Tsui, 1990: The automated tropical cyclone forecast system (ATCF). *Wea. Forecasting*, **5**, 653–660.

Navarro, E. L. and G. J. Hakim, 2014: Storm-centered ensemble data assimiliation for tropical cyclones. *Mon. Wea. Rev.*, **142**, doi:10.1175/MWR-D-13-00099.1.

NCL, 2014: The NCAR Command Language (Version 6.2.1) [Software]. Boulder, Colorado: UCAR/NCAR/CISL/VETS, http://dx.doi.org/10.5065/D6WD3XH5., http://dx.doi.org/10.5065/D6WD3XH5.

Nolan, D. S. and M. T. Montgomery, 2000: The algebraic growth of wavenumber one disturbances in hurricane-like vortices. *J. Atmos. Sci.*, **57**, 3514–3538, doi:10.1175/1520-0469(2000)057⟨3514:TAGOWO⟩2.0.CO;2.

Sampson, C. R. and A. J. Schrader, 2000: The Automated Tropical Cyclone Forecasting System (version 3.2). *Bull. Amer. Meteor. Soc.*, **81**, 1231–1240.

Tallapragada, V., et al., 2014: Hurricane Weather Research and Forecasting (HWRF) Model: 2014 scientific documentation (HWRF v3.6a). Development Testbed Center. [Available from http://www.dtcenter.org/HurrWRF/users/].

Uhlhorn, E. W. and D. S. Nolan, 2012: Observational undersampling in tropical cyclones and implications for estimated intensity. *Mon. Wea. Rev.*, **140**, 825–840, doi:10.1175/MWR-D-11-00073.1.

Willoughby, H. E. and M. B. Chelmow, 1982: Objective determination of hurricane tracks from aircraft observations. *Mon. Wea. Rev.*, **110**, 1298–1305.